



ACADÉMIE  
DES SCIENCES  
INSTITUT DE FRANCE

# *Comptes Rendus*

---

## *Physique*

Uwe Harlander , Michael V. Kurgansky, Kevin Speer and Miklos Vincze


**Baroclinic instability from an experimental perspective**

Published online: 30 September 2024

**Part of Special Issue:** Geophysical and astrophysical fluid dynamics in the laboratory

**Guest editors:** Stephan Fauve (Laboratoire de Physique de l'ENS, CNRS, PSL Research University, Sorbonne Université, Université Paris Cité, Paris, France) and Michael Le Bars (CNRS, Aix Marseille Univ, Centrale Marseille, IRPHE, Marseille, France)

<https://doi.org/10.5802/crphys.198>

 This article is licensed under the  
CREATIVE COMMONS ATTRIBUTION 4.0 INTERNATIONAL LICENSE.  
<http://creativecommons.org/licenses/by/4.0/>



*The Comptes Rendus. Physique are a member of the  
Mersenne Center for open scientific publishing*  
[www.centre-mersenne.org](http://www.centre-mersenne.org) — e-ISSN : 1878-1535



Review article / *Article de synthèse*

Geophysical and astrophysical fluid dynamics in the laboratory /  
*Dynamique des fluides géophysiques et astrophysiques au  
laboratoire*

# Baroclinic instability from an experimental perspective

*L'instabilité barocline d'un point de vue expérimental*

Uwe Harlander<sup>Ⓜ,\*</sup>,<sup>a</sup>, Michael V. Kurgansky<sup>Ⓜ</sup>,<sup>b</sup>, Kevin Speer<sup>Ⓜ</sup>,<sup>c</sup> and Miklos  
Vincze<sup>Ⓜ</sup>,<sup>d</sup>

<sup>a</sup> BTU Cottbus-Senftenberg, Dept. Aerodynamics and Fluid Mechanics,  
Siemens-Halske-Ring 15a, 03046 Cottbus, Germany

<sup>b</sup> A.M. Obukhov Institute of Atmospheric Physics, Russian Academy of Sciences,  
Pyzhevsky 3, 119017 Moscow, Russia

<sup>c</sup> Geophysical Fluid Dynamics Institute and Department of Scientific Computing,  
Florida State University, Tallahassee, 32306, FL USA

<sup>d</sup> Eötvös Loránd University Department of Materials Physics and HUN-REN-ELTE  
Theoretical Physics Research Group, Theoretical Physics Research Group, Budapest,  
H-1117, Hungary; Institute of Earth Physics and Space Science (HUN-REN EPSS),  
Sopron, H-9400, Hungary

*E-mails:* uwe.harlander@b-tu.de (U. Harlander), kurgansk@ifaran.ru  
(M. V. Kurgansky), kspeer@fsu.edu (K. Speer), mvincze@general.elte.hu (M. Vincze)

**Abstract.** In the mid-latitude atmosphere, synoptic eddies carry heat *and* momentum towards the poles and are hence a major element shaping weather and climate. The eddies are due to baroclinic instability caused by a supercritical vertical wind shear, which in turn is due to a supercritical meridional temperature gradient. Since the 1950s this crucial instability has systematically been studied with the thermally driven rotating annulus laboratory experiment. In this review, we summarize the research on baroclinic instability from the experimenter's perspective covering a period of about three quarters of a century. The fact that it was possible to tie in with the field of atmospheric dynamics, right from the start in the 1950s, makes the experiment unique compared to other experiments representing geophysical flow phenomena. The applications span a wide range of topics, e.g., regime transitions and the route to turbulence in the presence of rotation, or geostrophic turbulence, internal wave generation at baroclinic fronts, tests of operational weather forecasting methods, extreme value distributions with regard to climate, and more. In view of new measurement methods and data processing techniques, the baroclinic instability experiment will continue to be an important complement to numerical methods in the future.

**Résumé.** Dans l'atmosphère des latitudes moyennes, les tourbillons synoptiques transportent la chaleur et élan vers les pôles et constituent donc un élément majeur du temps et du climat. Les tourbillons sont dus

\*Corresponding author

à l'instabilité barocline provoquée par un cisaillement vertical du vent supercritique, lui-même dû à un gradient de température méridien supercritique. Depuis les années 1950, cette instabilité cruciale a été systématiquement étudiée à l'aide de l'expérience de laboratoire de l'anneau rotatif à entraînement thermique. Dans cette revue, nous résumons les recherches sur l'instabilité barocline du point de vue de l'expérimentateur, sur une période d'environ trois quarts de siècle. Le fait qu'il ait été possible d'établir un lien avec le domaine de la dynamique atmosphérique, dès le début dans les années 1950, rend l'expérience unique par rapport à d'autres expériences utilisées pour examiner les phénomènes d'écoulements géophysiques. Les applications couvrent un large éventail de sujets, par exemple les transitions de régime et la voie vers la turbulence géostrophique, la génération d'ondes internes sur les fronts baroclines, les tests de méthodes opérationnelles de prévision météorologique, les distributions de valeurs extrêmes en ce qui concerne le climat, etc. Compte tenu des nouvelles méthodes de mesure et des techniques de traitement des données, l'expérience sur l'instabilité barocline restera à l'avenir un complément important des méthodes numériques.

**Keywords.** Baroclinic instability, jet streams, Eady waves, Rossby waves.

**Mots-clés.** Instabilité barocline, courant-jets, ondes de Eady, ondes de Rossby.

**Funding.** HA 2932/8-1&2 (DFG); HA 2932/17-4 (DFG); PROCOPE (DAAD); State Assignment no. FMWR-2022-0011; Office of Polar Programs no. 1643679; Office of Polar Programs no. 1644172; Office of Polar Programs no. 2148517; OCE 1658479 (Ocean Science).

*Manuscript received 9 April 2024, revised 25 July 2024, accepted 5 August 2024.*

## 1. Introduction

Laboratory experiments in baroclinic instability are at least a century old now, and have been reviewed numerous times over the years, beginning perhaps with Fultz's [1] discussion of laboratory experiments as analogues of atmospheric motion. At the time, Fultz's experiments were stirring up ideas concerning the role of eddies in the thermal equilibrium of the planet [2] and Hide had embarked on a series of studies in the laboratory, first meant to reveal circulation related to Earth's dynamo, but soon applied to atmospheric motion [3]. These studies were to become the backbone of rotating annulus experimentation on baroclinic instability. Together with [4], the appearance of Fultz's [2] work and Eady's contemporaneous paper [5], providing an analytical result for the transition from axisymmetric flow to waves, where, in the context of the annulus, the Rossby radius of deformation is similar to the size of the tank, hints at the explosion of scientific effort on baroclinic instability in this postwar period.

While Hide's experiments drove quantitative investigation of the transition between regimes forward, from symmetric to steady or regular waves, quasi-periodic waves, vacillation and more chaotic regimes, Fultz's experiments appear to have helped convince the community of scientists studying weather and dynamics early on of the fundamental role of eddies. Judging from the language of the debate [6] the question of the relative role of the symmetric circulation versus waves in the transfer of heat from equator to pole was still an ongoing and acrimonious debate at the time. Fultz's description of some of his experiments were evidently directed to laboratory analogues of the Polar Jet, leaving open the more global question of multiple jets and eddy-driven cells, but in any case the function of baroclinic wave development and the associated meandering jet carrying heat "poleward" were deep insights to the thermodynamic systems operating in both the lab and atmosphere. The annulus experiment illuminated the notion of a dynamic, detached thermal boundary carrying heat meridionally in a dramatic fashion.

Later, by the time of Hide and Mason's [7] review, extensive previous work had, in their words, already occurred to map out the various regimes of baroclinic instability in the differentially heated rotating annulus. This mapping took place on the Taylor–Rossby number diagram (see Figure 1 and (2), (3) where the Taylor number is modified taking into account the aspect ratio.).

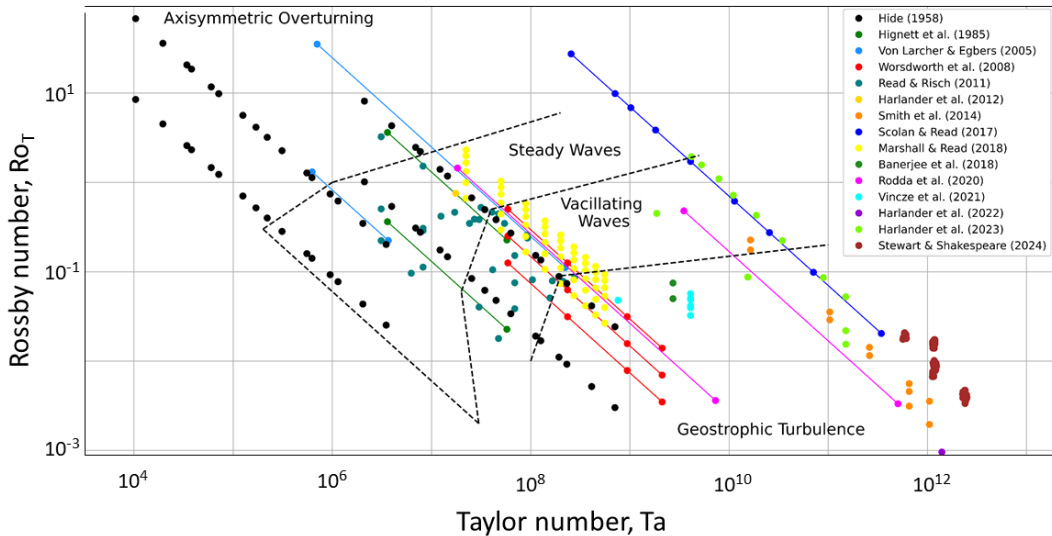


**Figure 1.** Regime diagram spanned by  $Ta$  and  $Ro_T$ . Data from different Hide experiments are shown (colored dots). Different flow regimes are indicated: axisymmetric (overturning) flow, steady waves, vacillating waves, and geostrophic turbulence. The Figure is an updated version of [9, Figure 2a].

Although it is important to note that variations in the exact definition of these parameters occur in the literature according to the laboratory configuration or the incorporation of related parameters, both of these parameters represent bulk properties of the system. Gent and Leach [8], on the other hand, performed experiments in an eccentric annulus with variable gap width and found azimuthally-dependent regimes. They made the observation that the parameters are locally important - that the flow structure is determined by local values of these parameters within the system.

In the time frame of the 1970 review [7], the Geophysical Fluid Dynamics Institute (GFDI) at Florida State University (FSU) was formed and devoted, in these early years, to the careful measurement of the time-dependent motion in the large rotating annulus, a new facility set up expressly for this purpose. GFDI publication number 1 by Pfeffer and Fowles [10] described wave dispersion induced by beating waves of nearby wavenumber and placed this evolution of the circulation onto the regime diagram. Some of the pioneers in the field of laboratory experimentation on baroclinic currents are pictured in Figure 2.

Interestingly, new work still refers back to these early experiments [11] in wave dispersion and vacillation. Subsequent efforts were made especially to quantify amplitude vacillation [12] and the role of topographic forcing [13] neglected in earlier experiments. Later work showed progress in the transition to turbulence [14] and led to the inference that that internal potential vorticity gradients – difficult to measure initially – needed to be more realistic [15]. The notion of an organized transition to turbulence took hold across many fields at the time and the annulus played an important role as a more geophysical representation of such phenomena.

This exciting new subject [16] literally brought chaos to the regime diagram and sharply redefined the role of irregular, quasi-periodic, and other notions under the heading of geostrophic turbulence. The area of transition to turbulence grew to dominate some efforts, for which the baroclinically unstable annulus was an attractive system to explore, more relevant to large-scale geophysical systems than say, Couette flow experiments. At GFDI, the modification of the annu-

lus to include 98 thermistors [17], and, following that, the additional technical achievements to produce an array of 2016 thermistors for a “synoptic network” in the large annulus allowed for a deeper analysis of internal structure and stratification through the transitions among regimes and toward geostrophic turbulence. Details of the vertical structure of waves and eddies, and wavenumber spectra evolution revealed time-dependent characteristics of both amplitude and structural vacillation and better defined turbulent, uncorrelated behavior at highly resolved detail. Früh’s [18] excellent review of these and related studies shows the richness of possible states found in the baroclinic annulus experiments, and foundational ideas about the feedback between internal flow and boundary layer structures.

Through these years of laboratory experiments with the rotating annulus, the application of the results was focused mainly on the atmosphere: the role of eddies, and the irregular, unpredictable nature of weather. With north-south continental boundaries that nearly span the globe the role of eddies and waves in the meridional circulation and transport of heat in the ocean was thought to be of a more secondary role. Moreover, the observational record from the ocean with respect to eddy motion lagged that of the atmosphere due largely to the difficulty making measurements from relatively slow-moving ships. But the circumpolar laboratory experiments with flow around Antarctica and the “dishpan” geometry of the Arctic Ocean make laboratory experiments with the baroclinic annulus-type configurations close analogies to these systems as well. Crucially, the deformation radius is so much smaller in the ocean relative to the size of the ocean basins that whole distinct regimes can “fit” into ocean basins, bringing back the notion of local parameters and local regime diagrams for individual oceans rather than a single planetary oceanic regime.

The record of ocean measurement expanded greatly in the 60’s and 70’s, partly as a result of the use of lagrangian techniques along with standard fixed point moorings. In parallel, laboratory experiments in baroclinic instability were also being carried out with the ocean in mind, to help explain observations that demonstrated the presence of Rossby waves (e.g. [19]) and turbulent mesoscale eddy motions in the ocean (The MODE Group, 1978; see also the review by [20]). Such efforts grew over time to help to comprehend instabilities associated with a vast range of conditions and ocean depths, and both convective and mean flow energy sources.

An early idealized experiment of lasting influence in the oceanographic community was that of Saunders [21], known as the cylinder collapse experiment, in which a volume of dense fluid was allowed to relax in a rotating container of slightly less dense fluid. This simple configuration, both relevant to the ocean and straitforward to model, generated vortices around the edge due to baroclinic instability. Maxworthy and Narimousa [22] carried out a series of experiments with a surface density or buoyancy flux and produced scaling arguments to demonstrate the evolution of these and related instabilities under forced conditions. A natural or “convective” Rossby number-like parameter  $R^*$  in these systems is based on a rotation length scale  $l_{rot}$

$$R^* = \frac{l_{rot}}{H}, \quad \text{where} \quad l_{rot} = \left( \frac{B_0}{f^3} \right)^{1/2}, \quad (1)$$

with the fluid depth  $H$ ,  $B_0$  the buoyancy flux, and  $f = 2\Omega$ , making apparent the notion of “slope” in sloping convection. While the traditional Rossby number is of order one in the initial state of these convective flows or plumes, the system rapidly evolves toward a dominantly geostrophic balance. Marshall and Schott [23] provide a comprehensive review of laboratory, field, and numerical work in this area of “open-ocean” convection and instability far from lateral boundaries.

While the advent of more effective and powerful numerical modeling techniques in the years following the heyday of annulus experiments dampened to some extent laboratory efforts, at least in the US as funding became more difficult to obtain for the larger technical groups needed

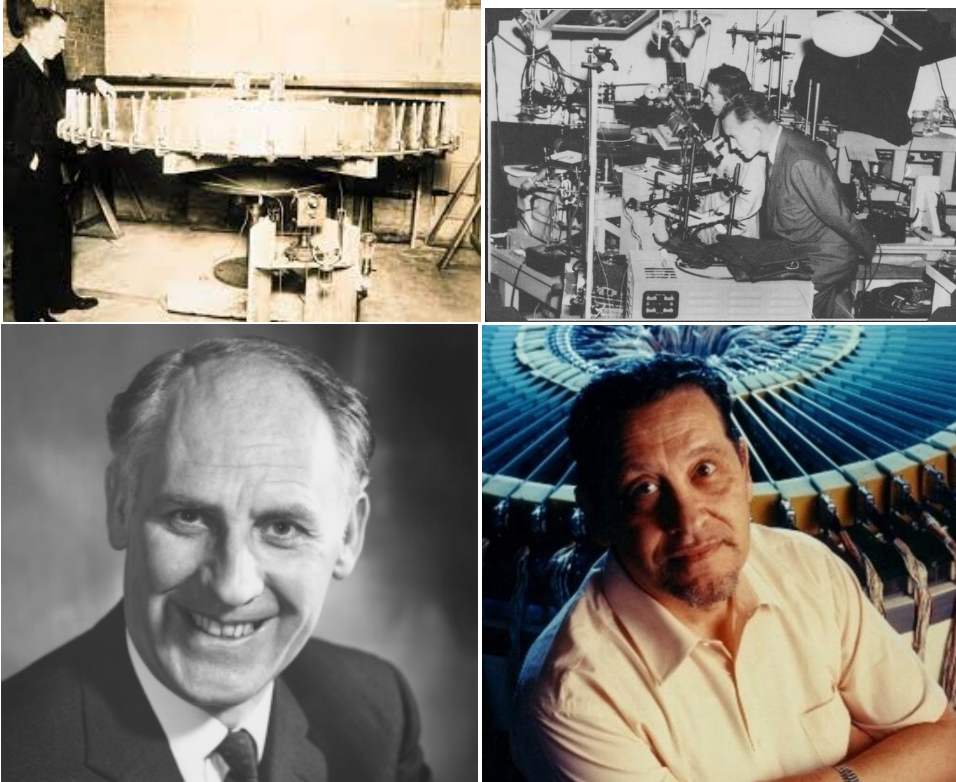


**Figure 2.** The pioneers (clockwise): Carl-Gustaf Arvid Rossby (Chicago), in front Dave Fultz (Chicago), Richard L. Pfeffer (Florida), and bottom left Raymond Hide (Oxford).

to maintain laboratory facilities, dedicated groups around the world remained very active. These and other later efforts are described in an exhaustive series of reviews by Read and associates [24–27], spanning the extension of laboratory experiments into detailed dynamical descriptions and analyses of the evolving time-dependent flow under various boundary conditions. The body of literature we can only touch upon here provide a broadly framed background to the history of the rotating baroclinic annulus and the vastness of the subject matter available in the laboratory. We are aware of shear-driven experiments (see the early experiments by J.E. Hart, e.g. [28] or the more recent studies by Lovegrove et al. [29] and Williams et al. [30]). Like the thermally driven rotating annulus systems, the mechanically driven open cylinder/annulus systems successfully reproduce the full range of flow regimes, and might allow for more direct verification of theoretical predictions in the laboratory. However, a two-layer density stratification is a very crude approximation to the structure of the atmosphere or ocean, and neglects the feedback of the flow on the stratification. Taking all this into account we focus here almost exclusively on the thermally driven variant. A thorough discussion of shear-driven experiments is well beyond the scope of this review.

New experiments are pointing to the continued relevance of the annulus experiment to climate change, and, for example, to extreme events in climate that may also have analogies in the laboratory [31], just as the early investigations were motivated by the idea of eddy fluxes in the atmosphere. The value of laboratory experiments as idealized testbeds for theory, parameterizations of complex heat, mass, and chemical property fluxes, and as inspiration and for the insight

they provide in and of themselves has not decreased over the years.

### 1.1. Governing Nondimensional Parameters

Returning to the earlier period, Fowles and Hide [32] listed as many as 18 nondimensional parameters for the rotating differentially heated annulus, some of them not independent, and in the end only a small subset of the total number turned out to be important. To find the *relevant* dimensionless parameters it is perhaps easiest to start with the underlying equations suitable for studying baroclinic waves in the Hide experiment. Considering the Boussinesq equations in a rotating frame of reference and nondimensionalizing the equations by scaling  $(\bar{x}, t, \bar{u}, p, T)$  with the factors  $(1/L, \nu/L^2, L/\nu, L^2/\rho\nu^2, \kappa/\nu\Delta T)$ , where  $L = b - a$  is the gap-width,  $a(b)$  the inner (outer) radius,  $\nu$  the kinematic viscosity,  $\Delta T$  the radial temperature difference, and  $\kappa$  the thermal conductivity, three nondimensional parameters appear in the dimensionless equations, the Rayleigh number  $Ra$ , the Taylor number  $Ta_L$ , and the Prandtl number  $Pr$

$$Ra = \frac{g\alpha\Delta TL^3}{\nu\kappa}, \quad Ta_L = \frac{4\Omega^2 L^4}{\nu^2}, \quad Pr = \frac{\nu}{\kappa}, \quad (2)$$

where  $g$  is the constant of gravity,  $\alpha$  the thermal expansion coefficient, and  $\Omega$  the angular velocity of the cavity rotation. Note that the Ekman number  $Ek$  can be written as  $Ek = 1/Ta_L^{1/2}$ . Hide and Fowles [32] modified  $Ta_L$  respecting different scales for the horizontal and axial direction,  $Ta = Ta_L L/d$ , where  $d$  is the fluid depth. In the literature on the baroclinic wave tank experiment it is common not to use the Rayleigh number but the so called thermal Rossby number, defined as

$$Ro_T = 4 \frac{Ra}{Pr Ta} = \frac{gd\alpha\Delta T}{\Omega^2 L^2}. \quad (3)$$

The latter corresponds to the classical Rossby number  $Ro = U/(\Omega L) = Ro_T$  when  $U$  is replaced by the thermal wind

$$U_T = \frac{gd\alpha\Delta T}{\Omega L}. \quad (4)$$

From the boundary conditions of the Boussinesq model two further geometrical parameters result, the radius ratio  $\eta_r$  and the aspect ratio  $\Gamma_d$

$$\eta_r = \frac{a}{b}, \quad \Gamma_d = \frac{d}{L}. \quad (5)$$

Note that the four parameters,  $Ta, Ro_T, Pr, \Gamma_d$  correspond with  $\Pi_5, \Pi_4, \Pi_6, \Pi_2$  in [32] and these parameters turned out to be most relevant in characterizing and comparing flows resulting from different annulus experiments. In fact, usually just  $Ta$  and  $Ro_T$  are taken to define the parameter space of the experiments. A recent example from [9] summarizing the parameters of Hide experiments covering a period from 1958 to 2024 is shown in Figure 1.

As discussed by [26], there are other nondimensional parameters that are relevant from a more physical point of view. One is the Burger number

$$Bu = \left(\frac{N}{2\Omega}\right)^2 \Gamma_d^2 = \frac{g\alpha\Delta T_\nu}{(2\Omega)^2 d} \left(\frac{d}{L}\right)^2, \quad (6)$$

a square of the product of the ratio between the buoyancy frequency  $N$  and the tank rotation frequency  $\Omega$  and the aspect ratio. Here  $\Delta T_\nu$  denotes the vertical temperature difference. According to the Eady model, this number needs to be small enough for baroclinic instability (see section 2.2 and 3.7.2). Read [26] calls this an ‘‘internal parameter’’ since it cannot be directly set by the experimenter. Note that the Froude number  $Fr$  is connected to the Rossby and Burger number via  $Fr = U/(Nd) = (Ro_T/2)/Bu^{1/2}$ . Assuming that  $\Delta T_\nu \approx \Delta T$  we find  $Fr \approx Ro_T^{1/2}/4$ , i.e.  $Bu = Ro_T/4$ .

For similarity between the experiment and planetary circulations,  $Ro_T, \Gamma_d$  need to be very small,  $Pr$  needs to be order one, and  $Ta$  needs to be very large. From figure 1 it is obvious that the

conditions are fulfilled for  $Ro_T$  and  $Ta$ ; however, in experiments with fluids like water or silicon oil,  $Pr$  is too large. This has an impact on the transition to instability and the complexity of the flow [33], but is not too essential for the process of baroclinic instability.

Figure 1 not only sorts experiments into the  $Ta - Ro_T$ -parameter space, it is also a regime diagram. Four different flow regimes are indicated: an axisymmetric regime without waves, a steady wave regime, a regime with vacillating waves, and a geostrophic turbulent regime. These regimes and the transitions between them have been discussed in detail, see e.g. [34]. There are further subdivisions into an upper and lower axisymmetric regime, into regimes with amplitude and structural vacillations, and a rich dynamics at the transition to geostrophic turbulence [24]. With the similarity parameters at hand, Read [26] and other authors connected these flow regimes to planetary circulation regimes.

## 1.2. The baroclinic wave experimental setup

The basic layout of the rotating annulus configuration and some of its variations are sketched in figure 3. Raymond Hide began his career using the annulus experiment at Cambridge in the 1950s, working on what was actually planned to be a simple laboratory model to study convection in the rapidly rotating fluid core of the Earth. The geometry of this experiment is shown in Figure 3, upper left picture [35]. The typical ‘‘Hide’’ tank is mounted on a turntable revolving around its axis of symmetry at angular velocity  $\Omega$  counterclockwise ( $\Omega > 0$ ) or clockwise ( $\Omega < 0$ ) and is divided into three sections by heat conductive co-axial cylindrical walls. The innermost cylinder (radius  $r = a$ ) is referred to as the ‘‘cold bath’’, where water of constant temperature usually below room temperature is circulated through a cooling thermostat (chiller). A separate regulated outer annular water circuit (radius  $r = b$ ) keeps the ‘‘warm bath’’ at a temperature larger than the one in the inner cold cylinder. The inner annular cavity of gap width  $L = b - a$  forms the experimental domain, and is filled up with the working fluid (air, water or oil) up to a certain height level. The fluid surface can be closed or is free, and the flow is driven by the

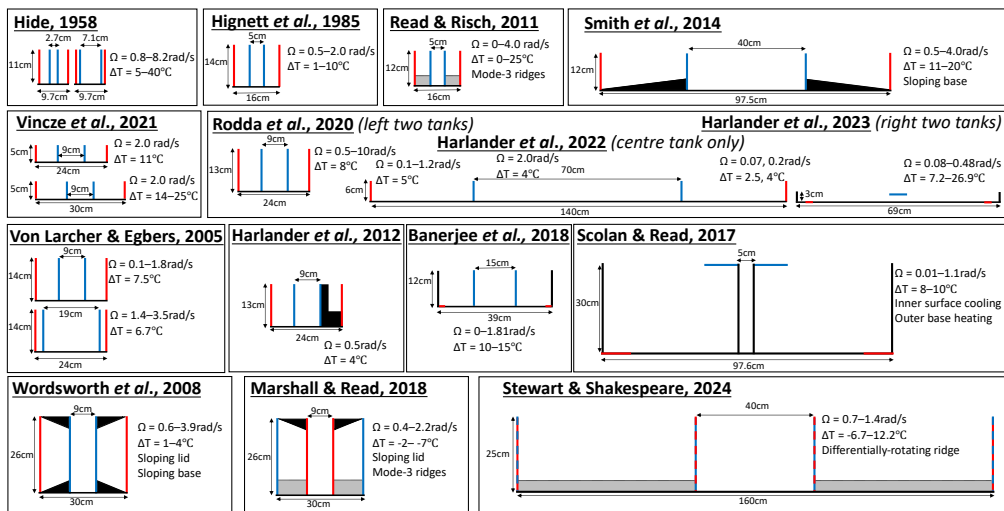


**Figure 3.** Geometries and setups for heating and cooling of baroclinic wave tanks from the period 1958 to 2024. The Figure is an updated version of [9, Figure 1].



buoyancy flux maintained by the temperature contrast  $\Delta T = T_b - T_a$  between the cylindrical walls. This configuration is a barebone representation of the atmosphere at the mid-latitudes of the Northern ( $\Omega > 0$ ) or Southern ( $\Omega < 0$ ) Hemisphere with the inner “cold” cylinder modeling the cold polar regions and the “warm” outer rim the subtropics.

As can be seen in Figure 3, there are several variations of the original Hide setup. Most notable is the use of a topographic  $\beta$ -plane [36, 37] allowing Rossby waves and the evolution of multiple jets or local topography [9, 37, 38] which partially blocks the flow or leads to interactions between stationary topographic waves and Rossby waves. The wide range of different geometries with a tendency towards larger tanks in more recent publications is also striking (compare the size of [35] and [9]). The aspect ratio  $\Gamma_d$  is  $\ll 1$  for tanks with a larger gap is hence somewhat closer to atmospheric conditions. Finally we mention variations with respect to the way the cavity is heated/cooled. Scolan and Read [39] did not cool and heat the walls but, in contrast, placed heat sources and sinks at the bottom and top such that Rayleigh–Bénard convection could take place close to the inner and outer wall. Hence local vigorous convection was possible in the “tropical” and “polar” regions of the annulus mimicking the situation of the atmosphere. In such a setup, in between the convective regions, stably-stratified baroclinic motion can still develop in analogy to the mid-latitudes of the Earth’s atmosphere. It was observed that, in contrast to the classical configuration, this alternative forcing typically exhibit more spatio-temporal complexity. This was confirmed by later studies [31, 40, 41].

As with the development towards more complex experiments and more complex questions to be answered with the experiments, the measurement methods used in the experiments also developed. In the early days, the focus was on flow visualisation. This was done, for example, with aluminium flakes floating on the surface [35]. Later, ink, Kalliroscope, Uranine and other substances were added as tracers, which, when illuminated with laser light, produced a fairly complete but only qualitative image of the flow (see Figure 8). Over the years, local flow measurements were done by using Laser Doppler Velocimetry and flow field measurements have been tackled by Particle Image Velocimetry (PIV), e.g. [11].

Temperature has been measured locally by temperature sensors or by arrays of thermocouple probes, e.g. [17, 42]. Surface temperature was measured using infrared cameras [43]. The lateral heat transport is an important variable to obtain insight into the eddy dynamics. The total heat transport was determined in the laboratory by real-time calorimetry of the regular baroclinic wave regime accessible in the rotating annulus up to the transition to geostrophic turbulence [44] and in some studies PIV and infrared thermography has been combined to measure the heat transport, e.g. [38].

Before reviewing applications of the annulus experiments in more detail in section 3, we start with a section on the theory of baroclinic instability.

## 2. Theory of baroclinic instability

At the beginning of the 20<sup>th</sup> century, in connection with the problems of applying fluid dynamics to natural environments, such as the atmosphere and ocean (now called geophysical fluids), it became necessary to consider models when the density  $\rho$  depends not only on the pressure  $p$ , but also on a second independent thermodynamic variable (in the case of two independent thermodynamic functions of state): either temperature  $T$  (in Kelvin) or specific (per unit mass) entropy  $s$ . In this more complex, but more realistic, model of a baroclinic fluid, the isobaric surfaces  $p = \text{const}$  and isopycnal surfaces  $\rho = \text{const}$ , generally speaking, no longer coincide with each other, but form an angle or “wedge”. In the presence of gravity and in the absence of general fluid rotation, the overturning circulation induced will tend to reduce this angle to zero. However, the presence of the Coriolis force inhibits this overturning motion (cf. [34]), and a

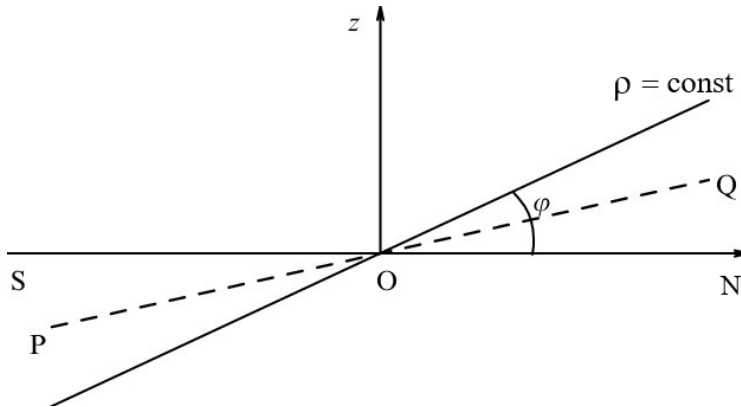


**Figure 4.** Disposition of isopycnal surfaces accompanying the baroclinic instability,  $\varphi$  is the angle of slope of surfaces  $\rho = const$  with respect to the horizontal.

non-zero angle is established between these surfaces in a rotating baroclinic fluid, promoting non-axisymmetric flows (“baroclinic waves”) of a general type sometimes called “sloping” or “slantwise” convection (ibid). According to the thermal wind equation, written here for a density-stratified, incompressible fluid

$$(2\vec{\Omega} \cdot \nabla) \vec{v} \approx \vec{g} \times \nabla \frac{\rho'}{\bar{\rho}}, \tag{7}$$

where  $\vec{\Omega}$  is the angular velocity of general fluid rotation,  $\vec{v}$  the velocity in a rotating reference frame,  $\vec{g}$  the acceleration due to gravity,  $\rho'$  the density deviation from the hydrostatically balanced value  $\bar{\rho}$ , this generally small angle is sustained by the effects of both background fluid rotation and vertical wind shear. Therefore, the baroclinic instability that arises in such a system and is reviewed in this article is equally characterized by the inhomogeneity of the density field on isobaric surfaces and by vertical shear of velocity. An important integral characteristic of the first of these factors is the available potential energy [45–47], which, stored in the basic flow, is used to supply the energy of disturbances during the development of baroclinic instability.

In fact, only trajectories of fluid parcels with slopes between the horizontal and the slope of the mean isopycnal surface can release the available potential energy and lead to generation of baroclinic waves. This is the classic “wedge of instability” argument (see [45]; and Figure 4).

Indeed, when a fluid parcel makes an excursion from point O to either point P or point Q, it will find itself in the ambience of fluid parcels with either smaller (in point P) or, respectively, larger (in point Q) density values. A appearing buoyancy force  $\vec{b} \approx \vec{g}(\rho'/\bar{\rho})$  will tend to move the fluid parcel at a greater distance from its initial position. Therefore, baroclinic instability is a specific form of thermal convection and is determined by the mutual configuration of the isopycnal and horizontal surfaces.

A major success of geophysical fluid dynamics in the 20<sup>th</sup> century was a rational explanation of why synoptic-scale atmospheric motions, particularly cyclones and anticyclones, have a dominant spatial scale of a few thousand kilometers, i.e., approximately an order of magnitude smaller than the scale at which energy is supplied from the Sun. This was a principal result of the theory of baroclinic instability pioneered by Charney and Eady [4, 5]. The main prediction was that the spatial scale of the fastest growing baroclinic disturbances (waves) is limited from below by the characteristic length given by the ratio between the buoyancy frequency times the vertical

length scale and the rotation frequency,

$$L_R = \frac{Nd}{\Omega} = \left( \frac{g\alpha\Delta T_v}{d} \right)^{1/2} \frac{d}{\Omega}, \quad (8)$$

known as the Rossby (internal or baroclinic) radius of deformation. Identifying the vertical temperature contrast  $\Delta T_v$  with the horizontal  $\Delta T$ , we find

$$Ro_T = \frac{L_R^2}{L^2} \quad \text{or} \quad Bu = \frac{Ro_T}{4} = \frac{1}{4} \frac{L_R^2}{L^2}, \quad (9)$$

with  $L$  the characteristic length-scale. Note that in laboratory experiments with mechanically driven baroclinic instability in a rotating tank (an open cylinder/annulus) filled with a two-layer fluid [28–30], an inverse parameter  $F = L^2/L_R^2$  is used, called the internal (rotational) Froude number. For a two-layer fluid  $L_R = (gd(\Delta\rho/\rho))^{1/2}/2\Omega$ , where  $\Delta\rho/\rho$  is the relative density difference between the layers.

For typical atmospheric conditions and a geographical latitude of  $45^\circ$ , the Rossby radius is slightly less than  $10^3$  kilometers. In the case of the ocean, this radius is (much) smaller and in high latitude regions it is even less than 10 kilometers.

### 2.1. Baroclinic instability and nonlinear stability analysis

In order to unify the presentation and keeping in mind applications to most geophysical fluid media, as well as to the laboratory experiment, we will proceed from the equations of motion of a density-stratified, incompressible fluid in a Coriolis force field in (a) the Boussinesq approximation and (b) the so-called traditional approximation, when the axis of general rotation coincides with the direction of gravity (vertical)

$$\frac{du}{dt} - fv = -\frac{\partial\Phi}{\partial x}, \quad \frac{dv}{dt} + fu = -\frac{\partial\Phi}{\partial y}, \quad \frac{dw}{dt} = -\frac{\partial\Phi}{\partial z} + b, \quad (10)$$

and

$$\frac{db}{dt} = 0, \quad \frac{\partial u}{\partial x} + \frac{\partial v}{\partial y} + \frac{\partial w}{\partial z} = 0. \quad (11)$$

A right-handed Cartesian coordinate system  $(x, y, z)$  is used, where in the case of geophysical media (such as the atmosphere and ocean) the  $x$ -axis is typically eastward, the  $y$ -axis northward, and the  $z$ -axis upward (opposite to the direction of gravity);  $(u, v, w)$  are the corresponding components of the fluid velocity. The Coriolis parameter, equal to twice the angular velocity of the general rotation, is presented as a linear function of the coordinate  $y$ :  $f = f_0 + \beta y$ , where  $f_0$  and  $\beta$  are constants. Let us recall that  $\Phi = \tilde{p}/\rho_0$ , where  $\rho_0$  is the constant (reference) value of density and  $\tilde{p} = p - p_0(z)$ , where  $p_0(z) = \text{const} - g\rho_0 z$  is the hydrostatic pressure corresponding to the reference state; the variable  $b = -g(\rho - \rho_0)/\rho_0$  is called buoyancy; here  $g$  is the acceleration due to gravity. In fact, this is the total buoyancy, which is further conveniently presented as the sum of the buoyancy corresponding to the average state of fluid stratification,  $\bar{b} = -g\bar{\rho}/\rho_0$ , and the deviation from it,  $b' = -g\rho'/\rho_0$ , assuming that  $\rho - \rho_0 = \bar{\rho}(z) + \rho'(x, y, z, t)$ . Similarly,  $\tilde{p} = \bar{p}(z) + p'(x, y, z, t)$ , where  $\bar{p}(z)$  and  $\bar{\rho}(z)$  are related by the hydrostatic relation, and we rewrite (1), explicitly highlighting the average stable state of the fluid

$$\frac{du}{dt} - fv = -\frac{\partial\Phi'}{\partial x}, \quad \frac{dv}{dt} + fu = -\frac{\partial\Phi'}{\partial y}, \quad \frac{dw}{dt} = -\frac{\partial\Phi'}{\partial z} + b', \quad (12)$$

and

$$\frac{db'}{dt} + N^2 w = 0, \quad \frac{\partial u}{\partial x} + \frac{\partial v}{\partial y} + \frac{\partial w}{\partial z} = 0. \quad (13)$$

In (12)  $\Phi' = p'/\rho_0$  and the square of the buoyancy frequency (Brunt–Väisälä frequency)  $N^2(z) = -g(d\bar{\rho}/dz)/\rho_0$  is considered a given function. For the atmosphere,  $N^2 = \text{const}$  is a good approximation away from the lower boundary, but in the ocean the profile  $N^2(z)$  is very inhomogeneous: the  $N^2$ -value takes on large values in the surface layer and the mid-depth pycnocline region and is small in the deeper layers of the ocean. In a laboratory experiment, when a continuous density profile is concerned, most often a linear decrease in density with height is reproduced, so that  $N^2 \approx \text{constant}$ .

The motions associated with baroclinic instability, to which this chapter is devoted, are characterized by the fact that hydrostatic and geostrophic relationships are satisfied to a good approximation. We represent the horizontal velocity field in the form  $(u, v) = (-\partial\Psi/\partial y, \partial\Psi/\partial x)$ , where  $\Psi = \Phi'/f_0$  is the geostrophic stream function, and in the quasi-static approximation  $b' = f_0(\partial\Psi/\partial z)$ . Since in the continuity equation the terms  $\partial u/\partial x$  and  $\partial v/\partial y$  cancel each other with asymptotic accuracy, the vertical velocity is very small and to a good approximation

$$\frac{d}{dt} = \frac{\partial}{\partial t} - \frac{\partial\Psi}{\partial y} \frac{\partial}{\partial x} + \frac{\partial\Psi}{\partial x} \frac{\partial}{\partial y}. \quad (14)$$

Therefore, eliminating  $\Phi'$  between the equations of the horizontal motion, we arrive at a system of two equations:

$$\frac{\partial}{\partial t} \nabla^2 \Psi + J(\psi, \nabla^2 \Psi + \beta y) = f_0 \frac{\partial w}{\partial z}, \quad (15)$$

$$\frac{\partial}{\partial t} \frac{\partial \Psi}{\partial z} + J\left(\psi, \frac{\partial \Psi}{\partial z}\right) = -\frac{N^2}{f_0} w. \quad (16)$$

Here,  $\nabla^2$  is the two-dimensional Laplacian in the  $(x, y)$ -plane and  $J(a, b) = (\partial_x a)(\partial_y b) - (\partial_y a)(\partial_x b)$  is the Jacobian. Eliminating the vertical velocity  $w$  between equations (15) and (16), we arrive at the equation for the conservation of quasi-geostrophic potential vorticity (in the case of fast annulus rotation and accordingly small Rossby numbers)

$$\frac{\partial q}{\partial t} + J(\psi, q) = 0, \quad q = \nabla^2 \Psi + \frac{\partial}{\partial z} \left( \frac{f_0^2}{N^2} \frac{\partial \Psi}{\partial z} \right) + f_0 + \beta y. \quad (17)$$

Equation (17) is solved with the boundary conditions of impermeability of the lower  $z = z_-$  and upper  $z = z_+$  boundaries of the fluid layer

$$\frac{\partial b}{\partial t} + J(\Psi, b) = 0, \quad b = f_0 \frac{\partial \Psi}{\partial z}, \quad z = z_{\pm}. \quad (18)$$

In the atmosphere, the earth's surface is chosen as the lower boundary  $z = z_- = 0$ , and the tropopause (where  $N^2$  experiences an upward jump) is taken as the upper boundary,  $z = z_+ = H$ . In the ocean, it is natural to take its surface  $z = z_+ = 0$  as the upper boundary, and the ocean floor as the lower boundary  $z = z_- = -D$ . In the atmosphere, the buoyancy can be considered proportional to the deviation of the potential temperature from the average value. In liquid media, including the typical laboratory experiment, we take the corresponding temperature deviation.

The general problem of nonlinear Lyapunov stability of a zonal (axially symmetric) flow may be considered under the  $\beta$ -plane approximation. If, initially, we consider a problem with axial symmetry, for example, about a laboratory experiment with a rotating cylindrical annulus, then an approximate theoretical analysis can be carried out in Cartesian coordinates, neglecting the effects of curvature of coordinate lines. This can be done when the corresponding centrifugal forces are much smaller than the Coriolis force (cf. [48]). The flow is assumed to be periodic in the zonal (azimuthal) direction, with a spatial period equal to the average circumference of the channel. The flow is limited laterally by vertical walls. We consider these walls impermeable to

fluid  $\partial_x \Psi = 0$ ,  $y = y_*$ ,  $y^*$ , and the velocity circulation on them being preserved for each altitudinal level,  $\int (\partial_y \Psi) dx = \text{const}$ ,  $y = y_*$ ,  $y^*$ .

We follow Arnold's [49] method, first applied by Blumen [50] for a nonlinear stability study of rotating and stratified Boussinesq fluid flows and use the existence in the problem of constants of motion: (a) energy

$$E = \frac{1}{2} \int \int \int \left( (\nabla \Psi)^2 + \frac{f_0^2}{N^2} \left( \frac{\partial \Psi}{\partial z} \right)^2 \right) dx dy dz, \quad (19)$$

as the sum of kinetic and available potential energy; (b) zonal (azimuthal) momentum

$$P = - \int \int \int \frac{\partial \Psi}{\partial y} dx dy dz, \quad (20)$$

and (c) Casimirs, whose conservation follows from (17) and (18):

$$F = \int \int \int \Phi(q, z) dx dy dz, \quad G = \int_{\Sigma_-} \int \Gamma(b) dx dy, \quad H = \int_{\Sigma_+} \int H(b) dx dy. \quad (21)$$

Here,  $\Phi, \Gamma$ , and  $H$  are arbitrary continuously differentiable functions, and  $\Sigma_{\pm}$  are the lower/upper end-walls at  $z = z_{\pm}$ , respectively. In the presentation, we follow [50–53].

Now a linear combination of constants of motion  $I = E - UP + F + G + H$  is formed, where an arbitrary constant  $U$  has the dimension of velocity. Let  $\bar{\Psi}(y, z)$  be a stationary zonal flow, the stability of which is being studied. Assuming the deviation  $\delta \Psi = \Psi - \bar{\Psi}$  to be small, let us expand  $I[\Psi] - I[\bar{\Psi}]$  into a series according to variations of successive orders:  $I[\Psi] - I[\bar{\Psi}] = \delta I + (1/2)\delta^2 I^2 + \dots$ . By properly choosing arbitrary functions  $\Phi, \Gamma$ , and  $H$  it is possible to arrange the series so that for a given  $\bar{\Psi}(y, z)$  at any value  $U$  the first variation  $\delta I$  becomes zero:

$$\begin{aligned} \Phi'_q |_{q=\bar{q}} &= \bar{\Psi} + Uy, \quad z_- < z < z_+, \\ \Gamma' |_{b=\bar{b}} &= \frac{f_0}{N^2} (\bar{\Psi} + Uy), \quad z = z_-, \quad H' |_{b=\bar{b}} = -\frac{f_0}{N^2} (\bar{\Psi} + Uy), \quad z = z_+, \end{aligned} \quad (22)$$

The prime at the top denotes differentiation and the subscript  $q$  means partial differentiation with respect to that variable. If we assume monotonicity of  $\bar{q}$  with the coordinate  $y$  for each  $z$ , and monotonicity of  $\bar{b}$  for  $z = z_{\pm}$ , respectively, then these conditions can always be satisfied. Calculating the second variation, we have

$$\begin{aligned} \delta^2 I &= \underbrace{\int \int \int \left( (\nabla \delta \Psi)^2 + \frac{f_0^2}{N^2} \left( \frac{\partial \delta \Psi}{\partial z} \right)^2 + \frac{(\partial \bar{\Psi} / \partial y) + U}{\partial \bar{q} / \partial y} (\delta q)^2 \right) dx dy dz}_A \\ &+ \underbrace{\int_{\Sigma_-} \int \frac{f_0}{N^2} \frac{(\partial \bar{\Psi} / \partial y) + U}{\partial \bar{b} / \partial y} (\delta b)^2 dx dy}_B - \underbrace{\int_{\Sigma_+} \int \frac{f_0}{N^2} \frac{(\partial \bar{\Psi} / \partial y) + U}{\partial \bar{b} / \partial y} (\delta b)^2 dx dy}_C. \end{aligned} \quad (23)$$

If all coefficients of the squared field variables are positive, then the zonal flow  $\bar{\Psi}$  is stable in the Lyapunov sense. This quadratic form is an exact conservation law (constant of motion) for equations linearized with respect to disturbances imposed on the basic flow, and represents a linear combination of pseudo-energy and pseudo-momentum.

What basic flows satisfy this stability criterion? To satisfy the necessary condition  $\delta I = 0$ , we assumed that  $\bar{q}$  is a monotonic function of  $y$ . The most natural step is to assume that this is a monotonically increasing function, similar to the Coriolis parameter  $f$ . Zonal winds in the atmosphere of mid-latitudes are predominantly westerly, i.e.  $\partial \bar{\Psi} / \partial y < 0$ . By choosing a constant  $U$  greater than the maximum velocity of the basic flow, we find that the volume integral in the first line of (23), the term denoted by A, is positive. This is formally analogous to the transition to a reference frame in which the zonal wind is easterly and the condition for positive definiteness of the volume integral is satisfied (cf. [49]). In the subtropical ocean, zonal currents are directed

to the east and the condition for positive definiteness of the volume integral is satisfied at  $U = 0$ . The problem is caused by the surface integrals in the second line of (23), the terms denoted by B and C. The potential temperature on the earth's surface decreases monotonically towards the poles, and the integral over the earth's surface, that is, the first term in the second line of (23), term B, is negative, so the second variation is indefinite in sign. The situation is aggravated by the integral taken over the upper boundary, that is, term C in the second line of (23). It is positive if the potential temperature decreases towards the poles, and negative in the opposite case. In any case, the quadratic form (23) is indefinite in sign, and the necessary condition for baroclinic instability is satisfied. If the potential temperature (buoyancy) changes very little at the lower and upper boundaries, then the surface integrals (term B and C) of (23) can be omitted. All that remains is the volume integral A of (23), and we arrive at the Charney–Stern criterion [54], originally derived using the normal mode approach for linearized quasi-geostrophic equations. This criterion states that a basic flow with a monotonically increasing potential vorticity is always stable. The important effects of the lower boundary were incorporated by Pedlosky [55] also using the normal mode approach; see [46]. This gives the Charney–Stern–Pedlosky necessary criterion for linear instability (see [47]).

An interesting case is when the potential vorticity can be considered constant at each height. This is a special idealization, acceptable when considering fairly narrow channels, when the Coriolis parameter can be considered approximately constant and this constancy can be extended to the entire quasi-geostrophic potential vorticity. Now, in (23), the last term in the integrand in the volume integral in the first line, term A, disappears and if the buoyancy has the same sign of growth at the upper and lower boundaries, then baroclinic instability is possible in the problem. Linear instability analysis in the Eady model [5] confirms this situation.

## 2.2. Linear stability analysis. Eady Model

The Eady Model is the most famous model in the theory of baroclinic instability, and it naturally fits the conditions of a laboratory experiment. A vast literature is devoted to it, including whole monographs. We will therefore limit ourselves to a brief formulation of the problem and a presentation of the key results. We assume the constancy of the Coriolis parameter,  $f = \text{const}$ , and of the buoyancy frequency,  $N^2 = \text{const}$ . For mathematical simplicity, we place the origin of coordinates in the middle between the rigid end-walls; then  $z_{\pm} = \pm H/2$ , cf. (18). The stream function of the basic flow, whose linear stability is being studied, is chosen, up to an insignificant additive constant, in the form  $\bar{\Psi} = -\Lambda yz$ . It corresponds to a flow with the velocity profile linear in height  $\bar{u} = -\partial\bar{\Psi}/\partial y = \Lambda z$  and the buoyancy field  $\bar{b} = f\partial\bar{\Psi}/\partial z = -f\Lambda y$ . The flow is considered within a channel with side walls at  $y = \pm L/2$ , on which the condition  $\Psi = 0$  is set.

Let us impose small disturbances on this basic flow and linearize equations (17), (18) with respect to them

$$\left(\frac{\partial}{\partial t} + \Lambda z \frac{\partial}{\partial z}\right) \left(\nabla^2 \Psi' + \frac{f^2}{N^2} \frac{\partial^2 \Psi'}{\partial z^2}\right) = 0, \quad (24)$$

and the boundary condition

$$\left(\frac{\partial}{\partial t} + \Lambda z \frac{\partial}{\partial x}\right) \frac{\partial \Psi'}{\partial z} - \Lambda \frac{\partial \Psi'}{\partial x} = 0 \quad \text{at } z = \pm H/2. \quad (25)$$

A class of disturbances of the normal mode type,  $\Psi' = \hat{\Psi}(z) \exp(ik(x - ct)) \sin ly$ , is considered. The wave number  $k$  is real;  $l = n\pi/L$ , where  $n$  is an integer; the parameter  $c$ , generally speaking, is complex and is a proper, spectral parameter of the problem. The basic flow is unstable if  $c$  has a positive imaginary part. Discarding the continuous spectrum of the problem, which does

not lead to instability, we arrive from (24) to the equation  $d^2\hat{\Psi}/dz^2 - (k^2/n^2)\hat{\Psi} = 0$ . Its general solution has the form

$$\hat{\Psi} = A \cosh \lambda z + B \sinh \lambda z, \quad \lambda^2 = \frac{N^2}{f^2} (k^2 + l^2). \quad (26)$$

Taking into account the boundary conditions, we have a system of two homogeneous equations with two unknowns  $A$  and  $B$ , which can be considered real. Equating the determinant of this system to zero, we obtain the characteristic equation for determining the eigenvalue  $c$

$$c^2 = \frac{\Lambda^2}{\lambda^2} \left( \frac{\lambda H}{2} - \coth \frac{\lambda H}{2} \right) \left( \frac{\lambda H}{2} - \tanh \frac{\lambda H}{2} \right). \quad (27)$$

Since  $\lambda H/2 > \tanh(\lambda H/2)$ , the value  $\alpha = \lambda H$  critical for instability is found from the equation  $\alpha_c = \coth(\alpha_c/2)$ , which has an approximate solution  $\alpha_c \approx 2.4$ . When  $\alpha > \alpha_c$  then the solution to the problem is a superposition of two neutral modes. For  $\alpha < \alpha_c$ , there are two complex conjugate imaginary roots, i.e. instability is long-wave in nature. The maximum growth rate of the unstable mode  $kc_i$  is achieved at  $n = 1$ , and moreover, we can further consider a wide channel so that  $l^2 \ll k^2$  and  $\alpha_{max} = \lambda_{max} H \approx 1.61$ .

The wavelength of the fastest growing disturbances is given by  $L_{max} = (2\pi/1.61)L_R$ . Here  $L_R = NH/f$  is the baroclinic Rossby deformation radius. The growth rate of this fastest growing mode is equal to (cf. [47])  $(kc_i)_{max} \approx 0.31\Lambda H/L_R = 0.31\Lambda f/N$ . This formula is widely used for estimations. Baroclinic instability is also referred to as sloping, or slantwise, convection in a Coriolis force field [34, 45, 47]. If the fluid motion is to release available potential energy, which is stored in a main zonal flow, and convert it into the perturbation kinetic energy, then fluid particle paths must have a slope between that of the surfaces  $z = const$  and  $b = N^2 z - f\Lambda y = const$ . For the Eady model the maximum rate of such a release is accompanied by the fluid particle path along the bisectrix of an angle  $\phi \approx \tan \phi = f\Lambda/N^2 \ll 1$  between the surfaces.

In Eady's model the horizontal spatial scale of the baroclinic instability  $L_*$  is set by the vertical scale  $H$  of the domain, unlike the Charney's [4] baroclinic approach for a semi-infinite domain with account for the beta-effect (cf. [47]). In Charney's model the vertical scale is defined by  $d^{-1} = d_\beta^{-1} + H_0^{-1}$ , where  $d_\beta = (f_0^2/N^2)(\Lambda/\beta)$  and  $H_0$  is the density scale height [45]. Here,  $f_0$  is a representative value of the Coriolis parameter. This means that if  $d_\beta \ll H_0$  then  $L_* = Nd_\beta/f_0$ ; if the inequality is reversed then  $L_* = NH_0/f_0$ . In Charney's model the maximal growth rate of unstable disturbances  $\sigma$  is of order  $\Lambda f_0/N$ , regardless of which vertical scale, either  $d_\beta$  or  $H_0$ , is used. It is also exactly the scale for the growth rate in Eady's model.

Above, the normal mode method was used for analysis. An alternative is the approach based on consideration of Eady edge waves, proposed in [56] and developed in [57, 58] (see also [53]). Baroclinic instability is interpreted as a result of the interaction of these edge waves. The results coincide with those obtained by the normal mode method, but some additional useful results are obtained. Thus, this approach allows us to estimate the phase shift between waves concentrated at the lower and upper boundaries, respectively. For maximally rapidly growing disturbances with  $\alpha_{max} \approx 1.61$ , this angle is  $\approx 47.8^\circ$  [53]. In addition, this approach allows us to determine the characteristics of optimal (fastest growing) disturbances. This refers to nonmodal transient disturbances with instantaneous growth rate which, in virtue of the nonnormality of the linearized dynamical operator, can on finite timescales exceed the growth rate of normal modes, and these transients can stay growing beyond the Eady cutoff scale [56, 59]. Unlike the normal mode method, the results significantly depend on the metric used: total energy, kinetic energy, potential energy on end-walls, etc. For two-dimensional disturbances (in the case of no dependence on  $y$ ) maximization of  $\gamma = E^{-1}(dE/dt)$ , where  $E$  is the total energy, cf. (19), shows that the maximum of  $\gamma_{opt}(\alpha)$  is achieved in the limit of long waves  $\alpha \rightarrow 0$  and  $\gamma_{opt}(\alpha)$  monotonically decreases along with an increase in  $\alpha$ . The line  $\gamma_{opt}(\alpha)$  touches the Eady normal

mode growth rate curve  $(kc_i)(\alpha)$  in a point  $\alpha \approx 1.915$ , which means that the normal mode is an optimal disturbance only for  $\alpha \approx 1.915$ , which exceeds  $\alpha_{max} \approx 1.61$ . In this case, the phase shift between the edge Eady waves is  $\approx 73.22^\circ$  [53]. In a more general approach, for a fixed point in time (optimization time), an initial disturbance is sought that maximizes the ratio  $F = E(t)/E(0)$ , where  $E(0)$  is the initial energy. In particular, for the optimization time  $t = 5(N/\Lambda f)$ , the wave number corresponding to the maximum energy ratio is equal to  $\alpha_{opt} \approx 1.2$ . Details are given in the review [53].

Taking into account Ekman friction at the lower and upper rigid end-walls is reduced to replacing the impermeability condition  $w' = 0$  with the condition  $w' = w_E = \pm(h_E/2)\nabla^2\Psi'$  at the end-walls at  $z = \mp H/2$ . Here  $h_E = (2\nu/f)^{1/2}$  is the thickness of the Ekman boundary layer, and  $\nu$  is the kinematic viscosity of the fluid. It is assumed that  $h_E \ll H/2$ . In this case, the characteristic equation for determining the eigenvalues is replaced by [34]

$$c^2 - 2ic \frac{\Lambda}{\lambda} F \coth(\lambda H) - \frac{\Lambda^2}{\lambda^2} \left[ \left( \frac{\lambda H}{2} - \coth \frac{\lambda H}{2} \right) \left( \frac{\lambda H}{2} - \tanh \frac{\lambda H}{2} \right) + F^2 \right] = 0. \quad (28)$$

Here,

$$F = \frac{1}{2} \frac{h_E N^2 (k^2 + l^2)}{k \Lambda f} \quad (29)$$

is the frictional parameter. When taking into account Ekman dissipation for the total energy  $E$  in the Eady model, cf. (19), we get the equation

$$\begin{aligned} \frac{d}{dt} \int \int \int \frac{1}{2} \left( (\nabla\Psi)^2 + \frac{f^2}{N^2} \left( \frac{\partial\Psi}{\partial z} \right)^2 \right) dx dy dz \\ = - \int \int_{\Sigma_-} f \frac{h_E}{2} (\nabla\Psi)^2 dx dy - \int \int_{\Sigma_+} f \frac{h_E}{2} (\nabla\Psi)^2 dx dy \end{aligned} \quad (30)$$

with a positive definite dissipative function; here, the levels  $\Sigma_\pm$  correspond to  $z = \pm H/2$ , respectively. As follows from this equation, for sufficiently deep annular containers, which are typically used in laboratory experiments, the influence of Ekman friction is relatively small [34].

At  $c \rightarrow 0$ , i.e. on the neutral stability curve if the principle of exchange of stabilities [60] is accepted, equation (28) reduces to the equality to zero of the expression in square brackets in (28). The minimum of the first term in these brackets is  $-0.09$  [61]. When  $F^2 < 0.09$ , there are two roots of this equation with respect to  $\alpha = \lambda H$ , which, according to [61], define the boundaries between the lower (upper) symmetric regimes and the wave regime, which are observed in the laboratory experiment.

When  $F^2 = 0.09$  then these roots merge and the critical value of the Ekman friction is given by

$$\frac{h_E}{H} = 0.3 \frac{\Lambda f L}{\pi N^2 H}. \quad (31)$$

In intermediate calculations, the most favorable value for instability  $l = \pi/L$  was used and it was also assumed that  $k = \pi/L$ , which maximizes the right side of (31). If following [61] we take  $(\Lambda f L)/(N^2 H) = 0.4$ , which is a reasonable choice for a laboratory experiment where this expression describes the ratio of the interior horizontal to the interior vertical temperature contrast, then the right side of (31) is equal to  $0.12/\pi \approx 0.04$ . It then follows from (31) that the baroclinic instability of an interior zonal flow is impossible if  $h_E/H > 0.04$  in the considered experimental setup.

In the above, we considered the analytically simplest symmetric case of two identical Ekman layers at the lower and upper end-walls. However, the asymmetric case of only one Ekman layer on the lower rigid end-wall and its absence on the upper free end-wall corresponds better to the conditions of the laboratory experiment. This more complex case was analyzed in [62]. In the same work, a model account was taken of the possible variation of the squared frequency of buoyancy  $N^2(z)$  in the Eady problem.



Rejecting the assumption  $f = \text{const}$  and accounting for the  $\beta$ -effect introduces significant mathematical difficulties into the problem, related with necessity to account for critical levels that correspond to  $\Lambda z - c = 0$ . This leads to the appearance of a countable set of weakly unstable normal modes. However, a numerical analysis shows that the growth rate of the fastest growing two-dimensional deep mode ( $l = 0, \alpha = O(1)$ ) is very insensitive to variations in the beta-effect. For example,  $(kc_i)_{\max} = 0.31\Lambda f/N$  at  $\gamma = 0$  and  $(kc_i)_{\max} = 0.286\Lambda f/N$  at  $\gamma = 10$  [63]. Here,  $\gamma = \beta HN^2/\Lambda f_0^2$  is the Charney–Green number [4, 63]. More details can also be found in [47] and [53].

Note that the surface quasi-geostrophic (SQG) model is conceptually close to the Eady model [64, 65]. For constant  $N$  and  $f$ , the analysis of instability within the framework of the Eady model can in fact be carried out starting from equation

$$\nabla^2\Psi + \frac{f^2}{N^2} \frac{\partial^2\Psi}{\partial z^2} = 0, \quad (32)$$

as was shown by [53].

### 2.3. Two-layer model

The simplest way to account for the  $\beta$ -effect in the problem of baroclinic instability is within the framework of the two-level Phillips model [66]. Here, we will consider a quasi-geostrophic model, consisting also of two layers of immiscible liquids but which may be a slightly closer analogue with respect to conditions of a laboratory experiment. The top layer has a thickness  $H_1$ , and the liquid in it has a density  $\rho_1$ . For the lower layer, such characteristics will be  $H_2$  and  $\rho_2$ , where  $\rho_2 > \rho_1$ . A reduced acceleration due to gravity  $g' = g(\rho_2 - \rho_1)/\rho_1$  is introduced. The equations of the quasi-geostrophic two-layer model are reduced to conservation laws ([47, p. 213])

$$\frac{\partial}{\partial t} q_i + J(\Psi_i, q_i) = 0, \quad i = 1, 2, \quad (33)$$

where

$$q_1 = \nabla^2\Psi_1 - m_1^2(\Psi_1 - \Psi_2) + f_0 + \beta y \quad (34)$$

$$q_2 = \nabla^2\Psi_2 + m_2^2(\Psi_1 - \Psi_2) + f_0 + \beta y + f_0 \frac{\eta_b}{H_2}, \quad (35)$$

with  $m_i^2 = f_0^2/(g' H_i)$ . Indices  $i = 1, 2$  refer to the upper and lower layers, respectively. In this case, in (34) the condition is used that the vertical velocity at the top of the upper layer vanishes (the “rigid lid” approximation); in (35) the function  $\eta_b$  describes the bottom topography. A systematic slope of the bottom, such that the effective thickness of the lower layer linearly decreases with increasing coordinate  $y$ , is mathematically equivalent to the beta effect. This is the basis for a practical way to model the beta effect in rotating containers.

For the basic flow that does not depend on the horizontal coordinates, the necessary condition for instability at  $\bar{u}_1 - \bar{u}_2 > 0$  has the form

$$m_2^2(\bar{u}_1 - \bar{u}_2) > \left( \beta + \frac{f_0}{H_2} \frac{d\eta_b}{dy} \right), \quad (36)$$

where it is assumed that  $\eta_b$  linearly depends on the coordinate  $y$ . In the case when  $H_1 = H_2 = H/2$  and  $d\eta_b/dy = 0$ , condition (36) coincides with what occurs for a two-level model if  $g' = HN^2/2$ . When  $\bar{u}_1 - \bar{u}_2 < 0$  the instability condition takes the form

$$m_1^2(\bar{u}_2 - \bar{u}_1) > \beta. \quad (37)$$

In both cases, instability requires vanishing either  $d\bar{q}_1/dy$ , cf. (34), or  $d\bar{q}_2/dy$ , cf. (35); see also [45]. The marginal stability curve at  $d\eta_b/dy = 0$  is given (in our notation) by the equation (see [45, p. 562])

$$\beta^2 (m_1^2 + m_2^2)^2 + 2\beta(\bar{u}_1 - \bar{u}_2)k^4 (m_1^2 - m_2^2) - k^4(\bar{u}_1 - \bar{u}_2)^2 (4m_1^2 m_2^2 - k^4) = 0. \quad (38)$$

If we substitute  $\bar{u}_1 - \bar{u}_2 = \beta/m_2^2$ , cf. (37) at  $d\eta_b/dy = 0$ , then the wave number at the minimum critical shear is equal to  $k_+ = (m_2^2(m_1^2 + m_2^2))^{1/4}$ ; at  $\bar{u}_1 - \bar{u}_2 = -\beta/m_1^2$ , cf. (14), it will be  $k_- = (m_1^2(m_1^2 + m_2^2))^{1/4}$  (ibid.). When  $m_1^2 = m_2^2 = m^2$  these formulas transform into the formula  $k = 2^{1/4}m$ .

A two-layer model targeted at the interpretation of laboratory experiment results was proposed in Lorenz [67]; see also [68, p. 222]). In this model, the stream function of the horizontal flow in the upper and lower layers of equal thickness  $H/2$  is  $\Psi + \tau$  and  $\Psi - \tau$ ; the buoyancy in these layers is  $\theta + \sigma$  and  $\theta - \sigma$ ; the velocity potential of the irrotational part of the horizontal flow in these layers is  $-\chi$  and  $\chi$ . If the Coriolis parameter  $f$  is constant and the static stability  $\sigma$  varies only with time, the equations of the model take the form

$$\frac{\partial}{\partial t} \nabla^2 \Psi + J(\Psi, \nabla^2 \Psi) + J(\tau, \nabla^2 \tau) = 0, \quad (39)$$

$$\frac{\partial}{\partial t} \nabla^2 \tau + J(\Psi, \nabla^2 \tau) + J(\tau, \nabla^2 \Psi) = f \nabla^2 \chi, \quad (40)$$

$$\frac{\partial}{\partial t} \theta + J(\Psi, \theta) = \bar{\sigma} \nabla^2 \chi, \quad \frac{\partial}{\partial t} \bar{\sigma} = -\overline{\theta \nabla^2 \chi}. \quad (41)$$

Here, a bar denotes a horizontal average. This system of equations is rendered closed by the thermal wind equation  $\nabla^2 \tau = (1/4)(H/f)\nabla^2 \theta$ . With neglect of the time variations of  $\bar{\sigma}$ , the system reduces to the two-layer Phillips model. An exact match is obtained by setting  $\theta = f(\Psi_1 - \Psi_2)/(H/2)$  and  $\bar{\sigma} = N^2 H/2$ .

Baroclinic instability has also been discussed for mean flows that depend on  $z$  and  $y$ , relative to disturbances that do not depend on the coordinate  $x$  along the flow, called symmetric baroclinic instability. A model with constant  $N$  and  $f$  has been discussed for an ideal fluid by [69]. Viscous and thermally conductive fluids have been studied by [48] and [70].

Finally we note that all the models discussed above were formulated in Cartesian coordinates. For application to the annulus the theoretical analysis has to be carried out in cylindrical coordinates. No surprises are to be expected with regard to the basic processes. However, due to the curvature of the streamlines in the cylindrical system, certain new effects may occur. It should also be mentioned that boundary layers, i.e. Ekman layers at the top and bottom boundaries and Stewartson layers at the vertical walls, influence the flow in the experimental cavity and might have an effect on the stability as well (see Section 3.7.1). In these regions quasi-geostrophic theory is not valid. Nevertheless, quasi-geostrophic numerical models have been rather successful capturing the essential features of experimental annulus data [71].

There may not be a direct comparison in the literature of all the theoretical results on baroclinic instability, which are discussed in this section, with experimental results on rotating annuli and their applications discussed in this review. However, fundamental theoretical results constitute the ideological basis of laboratory modeling, and theory and laboratory experiment complement and enrich each other. The third major player on this scene is the numerical modeling, which often helps establish a link between theory and laboratory experiment. For instance, numerical simulations of baroclinic wave flows in a rotating cylindrical annulus based on the Boussinesq Navier–Stokes equations, which form the basis of the quasi-geostrophic theory described in this section, have been successfully compared with laboratory measurement data (e.g., [72]).

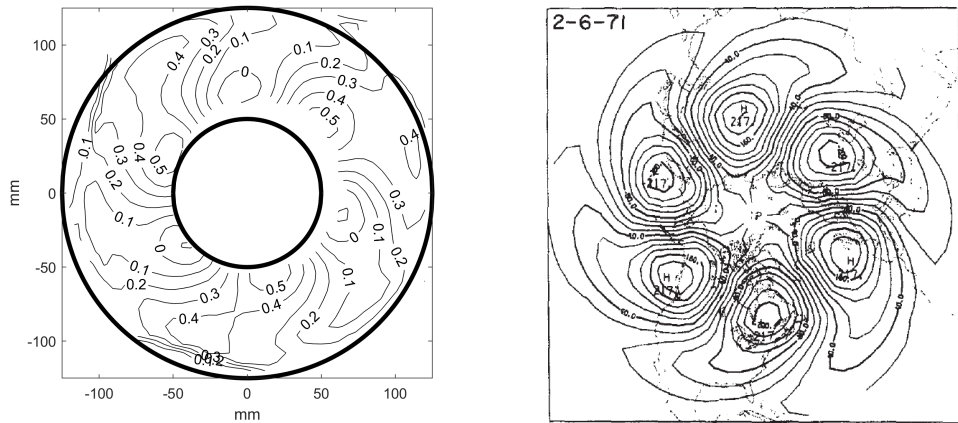


**Figure 5.** Fourier-analyzed 500hPa synoptic pattern of a state with maximum available eddy energy for wavenumber 3 (right), figure taken from [73] (with permission). Surface temperature anomaly (EOF1) measured at the BTU lab for  $\Delta T = 4$  K,  $\Omega = 4.8$  rpm,  $d = 13.5$  cm (left). The southwest-northeast ridge line tilt implies a northward/inward momentum transport.

### 3. Applications

#### 3.1. Flow regimes and heat flux

##### 3.1.1. Unblocked flow

A theory for the atmospheric general circulation should have at its center a theory for the eddy heat transport,  $\overline{v'T'}$ , where overbar means a zonal average, prime means a departure from the zonal average,  $v$  is the meridional velocity and  $T$  the temperature. Usually this transport is parameterized via  $\overline{v'T'} = -D\overline{T}_y$ , where the index  $y$  means a meridional derivative.  $D$  is a constant transport coefficient and it connects the transport with the meridional temperature gradient.  $D$  is, on the other hand, determined by characteristic length and velocity scales; however, it is not so obvious what these scales should be [74]. Moreover, the static stability is usually considered as a part of the background state but in fact it is a dynamic variable that varies strongly in space and time. The eddies in Earth's midlatitude atmosphere are part of the atmospheric *macro-turbulence* and at the end understanding this turbulence is essential for a theory of poleward heat transport.

The differentially heated rotating annulus is an experiment well suited to study and test ideas on the heat transport for different flow regimes and under different boundary conditions. As mentioned above, the experimental flow can be seen as an analog for atmospheric eddies and is therefore a good testbed for theoretical considerations on atmospheric flows. To illustrate this, Figure 5 shows an example of an atmospheric wavenumber 3 pattern of the 500hPa pressure level and a corresponding surface temperature pattern (EOF1) from an annulus experiment. The tilt of the patterns implies a northward/inward flux of momentum.

The heat transport in the annulus has been measured by [75], later by [44] and [76]. Without rotation but differential heating, the flow is restricted to boundary layers and a Hadley-type circulation can be observed. In the center of the cavity almost no motion can be seen and, in equilibrium, a stable vertical stratification is established. According to the experiments by [44] and [76], in this regime, the Nusselt number  $Nu$ , measuring the ratio between the total heat transport and the one by conduction alone, is about 13. When rotation is started, the thermal

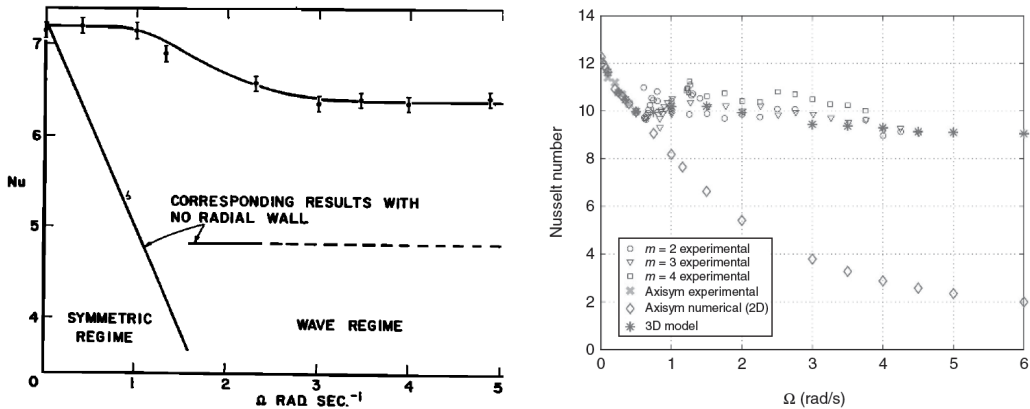


**Figure 6.** Left: A comparison of the variation of  $Nu$  with  $\Omega$  for the cases of a bounded and free annulus. Figure taken from [78] (with permission). Right: Experimental and numerical total heat transport. Figure taken from [25] (with permission).

wind (4) produces azimuthal flow components with a vertical shear. However, as long as the flow is axisymmetric (no baroclinic instability) the radial component needs to be ageostrophic since, due to azimuthal symmetry, there is no azimuthal pressure gradient. Hence, radial flow is mainly in the Ekman layers and in fact the meridional streamfunction looks similar as in the nonrotating case. However, the isotherms in the center of the cavity are sloping and the radial temperature gradient is enhanced there compared to the nonrotating case. In the experiments by [44, 76], for the axisymmetric regime with  $\Omega \neq 0$ ,  $Nu$  goes down to about 10 following a power law  $Nu \propto \Omega^{-3/2}$  (see Figure 6 (right)).

When rotation is further increased, the slope of the isotherms and the vertical shear in the bulk of the cavity increases and the azimuthal flow becomes baroclinically unstable (see the first transition in Figure 1). In the wave regime,  $Nu$  remains rather constant at about 10, no matter whether the azimuthal wavenumber is 2, 3 or 4. Compared with the decline of  $Nu \propto \Omega^{-3/2}$  for the hypothetical case of no baroclinic instability this is an amazing difference in the inward heat transport which is not fully understood from a theoretical viewpoint. Note that [44] suggested that the paper by [77] showed better agreement with the experimental results.

### 3.1.2. Blocked flow

There have been a number of experimental studies implementing a barrier in the annulus that fully or partly blocked the flow in the azimuthal direction [38, 78, 79]. For a complete blocking, as in the oceans, Bowden and Eden [78] pointed out that an azimuthal pressure gradient can exist and heat can then be advected due to a geostrophic boundary current along the barrier. In contrast to the free axisymmetric regime with a decline of  $Nu$  as  $\Omega^{-3/2}$ , no decline can be seen for the blocked flow (see Figure 6 (left)). For the latter, no regular wave regime exists and for larger  $\Omega$ ,  $Nu$  becomes somewhat smaller but remains constant when  $\Omega$  is further increased.  $Nu$  is larger for the blocked flow over the full range of  $\Omega$  considered. Similar results have later been found by [79].

The Antarctic Circumpolar Current is not blocked but has a prominent bottleneck, the Drake Passage. With a view on this situation, Harlander et al. [38] used a barrier that partially blocked the flow at the bottom and the inner wall. They measured the surface heat flux using velocity and temperature data for a single set of parameters in the wave regime. In that case baroclinic instability was present. However, the waves were not steady but showed a life cycle: downstream of the barrier the waves vanished but further downstream the waves recovered and reached

a steady state at the entrance of the narrows. The surface heat flux was computed from the combined PIV and surface temperature data with and without the barrier. The authors noticed that at the surface,  $Nu$  was almost an order of magnitude smaller with the barrier. Moreover, in the region where the baroclinic wave amplitude weakened, the radial heat flux was reversed and pointed from the inner to the outer wall. More recently, in a paleoclimate context, Vincze et al. [80] studied the effect of closing and opening the Drake Passage combining numerical modeling and lab experiments. This work is discussed in more detail in Section 3.6.

We note that experiments measuring the flow in the meridional plane of the baroclinic cavity are few in number (see Section 3.4 for Lagrangian data). However, numerical models suggest [31, 41, 81] that in the wave regime the meridional streamfunction can show a multi-cell structure depending on the aspect ratio  $\Gamma_d$  of the annulus. This will also alter the part of the heat flux related to the advection in the boundary layers.

### 3.1.3. Flux parameterization

The thermally driven rotating annulus is well suited to test parametrization schemes. Perez et al. [76] tested the mentioned closure for baroclinic eddy transport,  $\overline{v'T'} = -D\overline{T}_y$  numerically, but surprisingly found only a weak correlation between  $\overline{v'T'}$  and  $\overline{T}_y$ . A much better correlation was found between the potential vorticity flux  $\overline{q'T'}$  and  $\overline{q}_y$ . On the basis of the numerical data they were able to deduce the eddy diffusivity  $D_q$  using linear regression. In a further step, [76] implemented eddy parametrizations into numerical annulus models to check whether the models can reproduce data from DNS simulations. A more detailed review of these activities is described in [25].

Quite recently, using a two-layer quasi-geostrophic model, Gallet and Ferrari [82] developed a predictive scaling theory for the eddy kinetic energy, temperature fluctuations and the meridional heat flux of baroclinic turbulence. Later, this so called vortex-gas scaling regime was tested by applying a Boussinesq Eady model of baroclinic instability [83]. The authors showed that their predictions could be carried over from the quasi-geostrophic to the fully three-dimensional Boussinesq model. It would certainly be of great interest to test the scaling experimentally by using the annulus experiment, but this is a task for future research. We finally note that ideas for testing parameterizations for internal gravity waves using annulus experiments have been considered in [84].

## 3.2. Wave interactions, vacillations and turbulence

Linear stability theory describes well the onset of instability and it was successfully applied for explaining the typical  $Ta - Ro_T$ -stability diagram as shown in Figure 1, see also [34, Fig. 15]. However, after a short period of growth consistent with linear instability, the waves in a baroclinic cavity do not grow anymore but are saturated by nonlinear processes. This saturation does not necessarily result in a steady wave state. In fact, a regime of regular nonlinear oscillations strictly periodic in time, called vacillations, was discovered by [85] and [35], modeling baroclinic instability in a rotating differentially heated annulus. Hide [85] initially discovered what is now known as structural vacillation, or what was at one time called tilted-trough vacillation, e.g. [86], or wave shape (or form) vacillation [87]. Pfeffer and Chiang [86] and also Fowles and Pfeffer [88] made important advances in discovering amplitude vacillations, that is, vacillations in the amplitudes of eddies and not in the orientation of troughs and ridges (see [89] for an earlier and [18] for a later review). In the time that followed, attempts were made to detect a periodic, or quasi-periodic, regime in the analysis of real atmospheric data, which bears some resemblance to the zonal index cycle in the atmosphere (e.g. [90]). The observed oscillations of energy parameters in the atmosphere with a period of about 24 days and their connection with

baroclinic instability are described in [73]. Figure 5 (right) shows the wavenumber 3 geopotential height field at a state of maximum available potential energy and this state is in fact part of an atmospheric vacillation cycle. The minimum state occurred three weeks earlier and shows a similar pattern than the one displayed but with smaller amplitude and with maxima and minima that are shifted further towards the pole.

The occurrence of vacillations is an important feature of the nonlinear dynamics of perturbations of a basic baroclinic flow. This characteristic reflects the fulfillment of the energy conservation law in the adiabatic and inviscid case and is not related to the specific structure of the flow, cf. [53]. In this regard, the nonlinear oscillatory regime of flow instability in a two-layer quasi-geostrophic model was studied in [91], where the mechanism of occurrence of oscillations is described in terms of a time-periodic energy exchange between an unstable baroclinic wave and the background flow. For the two-level, quasi-geostrophic model of [67], which was assumed to be adiabatic and frictionless, Merlees [92] obtained an exact formula for the oscillation period (in terms of the complete elliptic integral of the first kind); this period, however, depends sensitively on the initial conditions. In a slightly dissipative case, the direct effect of dissipation on linear baroclinic instability is negligible, but dissipation can affect nonlinear oscillations in the long run (cf. [93]). Alternatively, on the attractor of a dissipative system, a kind of compensation of the effects of nonlinear instability and dissipation may occur, resulting in (almost) periodic oscillations (orbits), and nonlinear oscillations (vacillations) in a conservative system could serve as approximations for these orbits.

Here, we mention also the pioneering results of [94] on the existence of a limit cycle for small (but non-zero) viscosity in a quasi-geostrophic two-layer model at small deviations of the parameters from critical values. This type of oscillation has the desirable property that the ultimate oscillation is independent (in detail) of the initial conditions. Such vacillations are indeed observed in such (slightly) dissipative systems as the laboratory analogues of the atmosphere [12], although in laboratory experiments we are inevitably faced with a dissipative/forced fluid system. Nevertheless, the results obtained are qualitatively very similar to those obtained in the framework of conservative systems. If we consider that the occurrence of nonlinear oscillations (vacillations) is a consequence of the conservation of energy, then this similarity is explained by the exact conservation of energy for a conservative system and the energy conservation on average over the period of oscillation for a dissipative/forced system.

The line of research initiated by Pedlosky [91, 94] was further developed e.g. in [95] and in [96]. Pedlosky and Thomson [97] developed a weakly nonlinear theory of baroclinic instability of time-dependent flows, which exhibits finite-amplitude periodic oscillations of the limit cycle type when studying the nonlinear dynamics of parametrically unstable perturbations. Früh [18] reviews the amplitude vacillation in baroclinic flows based on experimental data, computational fluid dynamics, and low-order numerical models. The vacillation phenomenon, which occurs in various geophysical contexts, is addressed, e.g., in [98–101] and [102].

The above discussion mainly focused on amplitude vacillations, but for the route to irregular flows and geostrophic turbulence at higher rotation rates, structural vacillations are also important. Such vacillations have been described as an interaction between a small number of wave modes [67]. However, although mathematically elegant, this picture might not be complete. Ukajil and Tamaki [87] performed numerical simulation of structural vacillations in a rotating fluid annulus and revealed that the vacillations can be interpreted as the behavior of baroclinic waves affected by a weak barotropic instability. In view of the more irregular features observed in experiments with structural vacillations small-scale instabilities might also play a role (see also the discussion at the end of Section 3.7.4). The onset of structural vacillations is usually rather abrupt as was discussed by [103].

For higher rotation rates, the onset of structural vacillations is often a harbinger of the irregular flow state or geostrophic turbulence [14]. For the latter, energy power spectra show a slope between  $-3$  and  $-4$ . The shallower spectrum can be explained following the theory by [104], a steeper spectrum might be due to sharp fronts and filaments [105] that frequently occur in geostrophic turbulence. On the basis of data from annulus experiments, [106] studied spectral energy transfers and recently Rodda and Harlander [107] detected a power spectrum with slopes of  $-3$  for the large and  $-5/3$  for the small scales in an experiment with a small aspect ratio. However, the latter case was not in a turbulent regime. Read [25] stated in his review nine years ago that highly resolved experimental data on temperature and velocity are really needed to better understand energy exchanges in the turbulent regime and that is still true today.

### 3.3. *Jet streams*

Earth's atmospheric Polar Jet was an early motivation for laboratory experiments, as noted in the Introduction. The Subtropical Jet, and various oceanic interior jets, distinct from lateral boundary currents, raised further questions about their origins, relation to the general symmetric or "overturning" circulation in the oceanic context, and the relation to eddy forcing. From the early periods of experimentation to the present, interest in the banded structure of giant planets has also brought the concept of zonal jets into the foreground of research with the annulus.

Waves, eddies, and jet-like currents or streams are often present together in planetary atmospheres, oceans, and in the laboratory annulus experiments themselves. Sometimes the separation or distinction between these various circulation elements is not clear, or is confounded by variability, or depends on the interpretation of flow regime. The flow in wave regimes of the annulus, for example, recognized for connecting the inner and outer boundaries and for carrying heat meridionally (from an outer heat source to an inner heat sink for example), is analogous to jet streams in a portion of Earth's atmosphere. But this regime is not representative of jets in Earth's ocean, with its much smaller deformation radius  $L_R$  compared to basin size. The situation can be described by the basic thermal Rossby parameter of the system,  $Ro_T = L_R^2/L^2$ , see (8) with  $L$  the characteristic length scale, where the oceanic regime is represented by a smaller value of  $Ro_T$ . Note that the Taylor number in the ocean is far larger than that in the laboratory, but laboratory results suggest that after transition to the geostrophic turbulence beyond a value of about  $10^8$ , the regime is relatively independent of  $Ta$ .

The organization of the turbulent regime into quasi-zonal jets relies on the  $\beta$ -effect. The sloping surface of rotating tanks, either free or with a lid, provides a topographic beta-effect, investigated early on by [108], and more thoroughly by [106] into the stronger nonlinear flow regimes. While there is skepticism concerning the representation of  $\beta$  by a sloping upper or lower boundary, since it does not produce a true interior mean vorticity gradient, experimental results clearly imply an important effect. That small-scale convective motion, generated by either cooling at the surface or heating from below, can also lead to larger scale baroclinic flow structure including jets was developed in experiments by, for example, [109]. Their experiment used a parabolic bowl to produce a net thickness gradient, or potential vorticity gradient, and gave rise to azimuthal jets. Experiments on the large table at Grenoble, also forced with small-scale convection, showed that jets were produced consistent with a generation mechanism by Reynolds stresses [110].

The recognition of the role of jets in the ocean arising from baroclinic instability was slower to develop. Eventually, observations showed deep zonal jet structures with several candidate mechanisms, including the baroclinic instability of the meridional flow [111]. Modeling efforts also suggested alternate explanations not involving baroclinic instability via the arrested decay of long Rossby waves [112]. Similar to the case of small-scale forcing of larger scale flow structures

in the laboratory, interior mixing in the presence of topography has been implicated as well in the development of zonal jets [113].

In experimental configurations with a beta-effect, the introduction of a Rhines length scale,  $L_\beta = (U/\beta)^{1/2}$ ,  $U$  being a characteristic eddy velocity, produces another parameter,  $L_\beta^2/L^2$ , where  $L$  is the annulus' gap width, that becomes useful for distinguishing the regimes for which jets appear in the baroclinic annulus. In the laboratory setting, [36] showed multiple jet structure in an annulus in a regimes with small values of this parameter, thought to be relevant to the largest and broadest zonal flow in the ocean, the Antarctic Circumpolar Current, present in the circumpolar open channel between Antarctica and the southern continents. This current system is known to be composed of multiple zonal jets, as many as ten or so, typically with one or two dominant at any particular time and place. Intermittency and meridional jet migration characterize the longer time evolution of this system [36]. We note finally that multiple jet formation has also been studied experimentally using a mechanical forcing [114].

Multiple jets in baroclinic flow resolved in the annulus have become profoundly relevant paradigms for circulation in Earth's ocean and atmosphere, and on other planets as well. For additional background and newer developments see the review on jets in this collection.

### 3.4. Chaotic transport

Lagrangian or chaotic transport is of interest in any branch of geophysical fluid dynamics in which the transport and mixing of fluid, fluid properties, and material moving in the fluid is relevant. The theory was developed as part of dynamical system theory and later applied to different fields in physics including fluid mechanics. In our context, transport properties in a meandering jet are in the center of attention. The Gulf Stream and the intense flow connected to the polar vortex are examples of meandering jets that show many features in common with the flow in the baroclinic wave experiment.

The motion of passive particles, not affecting the flow, follow the equation

$$\frac{d\vec{x}}{dt} = \vec{v}(\vec{x}, t), \quad (42)$$

where  $\vec{x} = (x, y, z)$  is the particle position in the 3D space and  $\vec{v} = (u, v, w)$  is the velocity vector in this space. For a given velocity, solutions of (42) are the trajectories of the particles. Note that invariants of adiabatic flows like potential vorticity or potential temperature (or temperature in Boussinesq models) can be considered as tracers as well, however, they are not passive since they affect the flow.

In the bulk of the fluid within a baroclinic wave tank the flow is nearly 2D. Then we can introduce a streamfunction  $\psi(x, y, t)$  and write

$$\frac{dx}{dt} = u(x, y, t) = -\frac{\partial\psi}{\partial y}, \quad \frac{dy}{dt} = v(x, y, t) = \frac{\partial\psi}{\partial x}, \quad (43)$$

where  $\psi$  is a Hamiltonian and  $x$  and  $y$  the canonically conjugated variables [115]. In this case, chaotic transport can be studied by the methods from Hamiltonian dynamics.

To illustrate particle transport within a 2D meandering jet we consider the following streamfunctions

$$\psi(x', y, t) = cy + \psi_0 \left( 1 - \tanh\left(\frac{y - y_c}{\lambda / \cos \alpha}\right) \right) + \epsilon \psi_1(x', y, t), \quad (44)$$

with  $y_c = A \sin kx'$ ,  $\alpha = \tan^{-1}(Ak \cos kx')$ ,  $0 < \epsilon < 1$ , and

$$\psi(x', y, t) = cy + \psi_0 y_c \sin y + \epsilon \psi_1(x', y, t), \quad (45)$$

where  $x'$  is in a reference frame that moves with the constant speed  $c$ , i.e.  $x' = x - ct$  and  $k$  is a zonal wave number. The amplitudes are constant and are denoted by  $\psi_0$  and  $A$ . Here  $\psi_1$



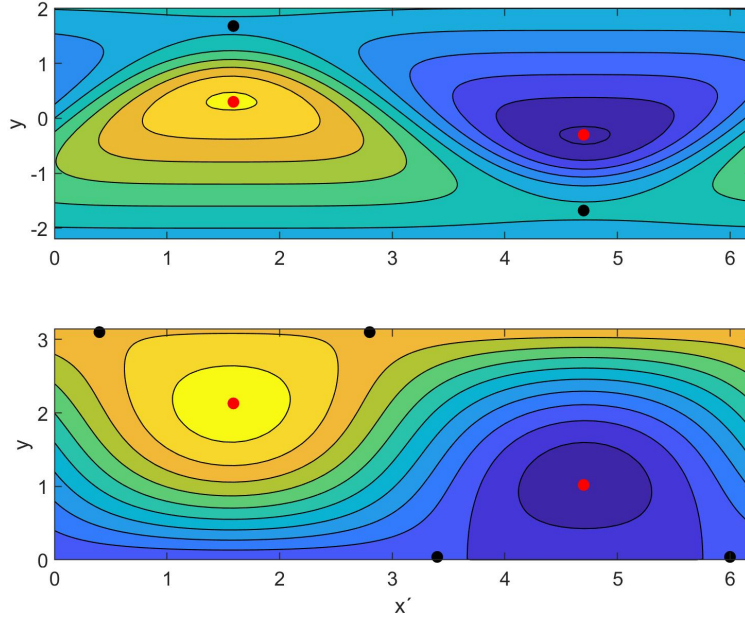


**Figure 7.** Two meandering jets, one localized in an open shear flow (top) (44), and one in a channel with walls oriented in the zonal direction (45). The black dots are hyperbolic (saddle) fixpoints, the red dots elliptic (oscillatory center) fixpoints. We used  $k = A = \psi_0 = 1$ ,  $c = 1/2$ ,  $\lambda = \pi/6$ , and  $\epsilon = 0$ .

is a time dependent perturbation of the primary wave. The former jet (44) corresponds to a localized meandering jet in an open shear flow [116] (see Figure 7, top), the latter one (45) to a meandering channel flow with walls oriented in the zonal direction [117] (see Figure 7, bottom). These examples are in a sense “clinical” versions of realistic jets for which a mathematical analysis is simpler than for its real counterparts.

The dots in Figure 7 mark fixpoints, i.e. points at which the left hand side of (43) vanishes. The red dots denote elliptic center points, surrounded by closed streamlines. In contrast, the black dots stand for hyperbolic saddle points located on streamlines that separate regions of meandering and circulating flows. In the reference frame in which the flow is displayed in Figure 7, the streamlines correspond with trajectories. Streamlines separating meandering and circulating flows are hence *transport barriers* for the flow: fluid exchange between the two regions is impossible since no trajectories can cross the transport barrier that itself is formed by a flow trajectory.

Transport barriers play a fundamental role in atmospheric as well as oceanic sciences. For example, mixing events at the edge of the Antarctic polar vortex play a key role for the transport of ozone and heat in this region [119, 120] and thus have an impact on the southern hemisphere weather and climate [121]. In such large-scale vortices potential vorticity (PV) can be used as a tracer [122]. Transport barriers for PV are related to steep PV gradients found at the edge of the polar vortex. The same steep gradients occur in mid-latitude jets making meridional PV exchanges difficult. Spreading of pollutants play an important role in the global ocean. Forecasting the motion of polluted water, e.g. following an oil spill is essential to keep environmental damage within limits and in this context transport barriers are very relevant [123]. A recent extensive review on transport barriers is given by [124].

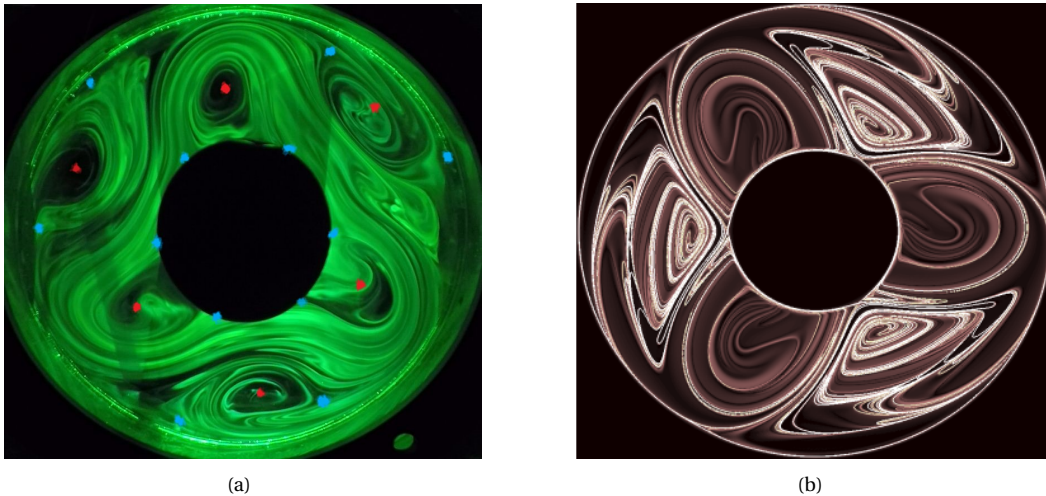


**Figure 8.** a) Uranine visualization of a wavenumber 3 baroclinic wave at depth 1 cm from the surface. For this visualization experiment, the tank revolution was  $\Omega = 5$  rpm, and the temperature difference was  $\Delta T = 4$  K. Center points are given in red, saddle points in light blue. b) Contour lines of  $\|\nabla M^{(b)}\|$  showing attracting material curves computed at initial time  $t_0 = 0$ s and  $\tau = 6600$ s. The calculations are based on the kinematic model developed by [118] using PIV velocity and temperature data from the experiment shown in a). A perturbation has been applied to the kinematic model that leads to a break up of the transport barriers. Figure taken from [118] (with permission).

Mixing events can be triggered by adding time dependence in the streamfunctions (44), (45), i.e. by using  $\epsilon \neq 0$ . For mixing, the saddle points marked as black dots in Figure 7 have a very significant meaning. The reason is that streamlines intersecting with saddle points are either so called stable or unstable material manifolds (also called hyperbolic manifolds). These hyperbolic manifolds mark regime boundaries. In the case sketched in Figure 7 we see either a meandering jet regime or vortex regime with closed streamlines. The hyperbolic manifolds break up when  $\epsilon$  is nonzero and the streamfunction becomes time dependent. Then mixing takes place along the hyperbolic manifolds close to the saddle points.

The mixing and its connection to saddle points can be observed in the baroclinic wave tank. Figure 8(a) shows an example of a baroclinic wave with azimuthal wave number 3. Center points are given in red and saddle points in light blue. The two flow regimes, vortex flow and meandering jet, can clearly be distinguished. However, fluid mixing has obviously taken place and this is due to (a weak) time dependency and a breakup of hyperbolic manifolds close to the blue points. It is easy to recognize that the flow shown as an example corresponds to the streamfunction (45), displayed in Figure 7 (bottom). The straight channel displayed has wave number 1 (4 saddle points) in contrast to the wave with wave number 3 ( $3 \times 4$  saddle points) in the annular channel of Figure 8(a).

Apart from these rather theoretical considerations, mixing in jet streams has also been the subject of intensive experimental research. Sommeria et al. [125] studied the transport of particles in a barotropic jet. The jet was produced in a rotating annulus with sources and sinks at the bottom. The bottom had conical shape to mimic a  $\beta$ -plane. The jet results from an instability due to the radial shear of the flow. The initially unstable jet profile is first broadened due to barotropic instability until it is stabilized by the beta effect. The sources and sinks in the annulus create a steep PV gradient in the jet's center forming a transport barrier for tracers. Using the

same experimental apparatus, Behringer et al. [126] heuristically fitted a kinematic model to the experimental data. Then they studied how transport barriers depend on the number of waves included in the model, and found that the addition of a third wave can break the transport barrier if the wave amplitudes exceed the width of the jet.

In addition to the consideration of jets caused by barotropic instability, three-dimensional jet streams formed by baroclinic instability have been studied using a differentially heated rotating annulus (see Figure 3). Saguta and Yoden [127] numerically studied Lagrangian motion in a steady baroclinic annulus wave. They subdivided the Lagrangian flow into different regions: the upper-level and lower-level jets, the cyclonically and anticyclonically trapped regions, and the inner, outer and lower boundary layers. Although the particle paths always showed some chaotic behaviour, the particles usually visit these regions in an organized way. However, inside the cyclonic and anticyclonic vortices particles were usually not found implying that these regions were separated from the flow by transport barriers. Interesting also is the Lagrangian view of the heat transport. The fluid particles absorb heat at the heated outer boundary layer and release it at the inner cooled boundary layer. In between, they carry the heat without much loss.

Later, Tajima et al. [128] tried to reproduce the numerical findings by experiments inserting ink at different positions in a steady baroclinic wave field. They found that the structure of the cyclonic and anti-cyclonic vortices are composed of a well-isolated core region but split into separate upper and lower layers. Next to the core a transition zone was found where fluid particles can travel towards and from a vortex' outside but usually not to its core region. A more quantitative view on chaotic trajectories in the 3D baroclinic wave flow was taken by [129]. Many features observed by [127] could be experimentally confirmed. However, from the tracking data alone it was not possible to derive measures for transport and mixing on the basis of the chaotic particle motions.

Keane et al. [130] showed that finite scale Lyapunov exponents (FSLEs) are useful to find boundaries between different regions of the differentially heated rotating annulus flow identified earlier by [127]. Keane et al. further considered Eulerian symmetry measures (ESMs) as an alternative or supplement to FSLEs. Very recently, Agaoglou et al. [118] quantitatively constructed a kinematic model (43) from simultaneous measurements of the temperature and the horizontal flow of a baroclinic wave experiment. In time-dependent dynamical systems stable and unstable manifolds as well as the structures around elliptic center points can be visualized by using Lagrangian Descriptors (LDs). This diagnostics has been introduced by [131] and was first applied in ocean dynamics. The LD that was used in [118] was the  $M$ -function defined as

$$M(\mathbf{x}_0, t_0, \tau) = \int_{t_0 - \tau}^{t_0 + \tau} \|\mathbf{v}(\mathbf{x}(t), t)\| dt, \quad (46)$$

where the norm  $\|\cdot\|$  measures the length of the velocity vector and  $\tau$  denotes the integration time. At a given initial time  $t_0$ , the function  $M(\mathbf{x}_0, t_0, \tau)$  measures the arclength that is traced by the trajectory starting at  $\mathbf{x}_0 = \mathbf{x}(t_0)$ . The  $M$  function is powerful tool to disentangle a complex dynamics and this approach has many applications in oceanic and atmospheric sciences. A review can be found in [132]. The integral in (46) can be divided into two parts,  $M = M^{(f)} + M^{(b)}$ . The first term integrates from  $t_0$  to  $t_0 + \tau$  and the second from  $t_0 - \tau$  to  $t_0$ . The forward component,  $M^{(f)}$ , elaborates structures of stable manifolds, and  $M^{(b)}$ , can find structures of unstable manifolds. In [118] the interest was on attracting material curves and the analysis was restricted to  $M^{(b)}$ .

Figure 8 (b) highlights singular features in  $\|\nabla M_b\|$ , the modulus of the gradient emphasizing singularities in  $M^{(b)}$  even more clearly. Singular features in  $M$  are associated with the existence of invariant unstable manifolds. In Figure 8 (b), Agaoglou et al. [118] used  $\tau = 600$  s and applied

a perturbation to the kinematic model. This perturbation allows for mixing across the jet by destroying invariant tori.

Dye dispersion processes in geostrophic turbulence were studied using rotating annulus experiments by Jánosi et al. [133], in the thermal Rossby number range of  $Ro_T = 0.01-0.1$ . In each run a 1 ml drop of standard fluorescent dye was injected at the water surface, and its dispersion was evaluated from video recordings taken from above, by determining the total area covered by the dye cloud, and its azimuthal extent as a function of time. The results were compared with passive tracer propagation simulations driven by global reanalysis wind fields (i.e. semi-empirical wind fields, based on measured data but interpolated to achieve uniform global coverage). They found that in this irregular wave regime the horizontal extent of the tracer cloud increases linearly in time (Batchelor scaling) for intermediate timescales (“weeks”) in the atmosphere and in the experiment as well.

### 3.5. *Blocking*

In meteorology, the term “atmospheric blocking” describes the formation and development of large-scale high pressure patterns in the midlatitude troposphere that are nearly stationary, highly persistent and block or redirect migratory cyclones. This causes long-term weather anomalies, heat waves and draughts in summer and cold spells in winter, and has profound impact on midlatitude weather and climate conditions, not only over the region in which the blocking occurs but over upstream and downstream areas as well.

The axis of blocking highs (blocks) usually has a slight tilt with height, i.e. blocking highs are, to a good first approximation, barotropic structures. However, the existing small tilt provides feeding of blocking highs not only due to migratory eddies (cyclones and anticyclones) [134], but also at the expense of the available potential energy stored in the main zonal flow [135], i.e. due to the action of baroclinic instability.

In Charney and Straus [136], by generalizing the work [137] to the case of a baroclinic atmosphere, a two-layer atmospheric model was considered taking into account the orography of the Earth. The highly truncated solution of the governing quasi-geostrophic equations, by using the Galerkin method, was shown to allow multiple equilibria, associated with resonantly forced Rossby waves, one of which corresponds to the atmospheric blocking. Maintaining this blocking state requires large values of the equator-pole temperature difference  $\Delta T$  and is associated with both the so-called orographic (form-drag) instability, which is already present in the barotropic atmosphere [137], and with the baroclinic instability of the main zonal flow.

A competing point of view on the mechanism for the forcing and supporting a blocking high treats it as a regional phenomenon forced by migratory cyclones and baroclinic energy conversion [138]. To the major extent this corresponds to dipole-type [139] and omega-type blocking [140]. A conceptual model of these two types of blocking in terms of correspondingly a pair (dipole) and a system of three (tripole) Kirchhoff point vortices was introduced in [141] and further developed in [142] and [143]. There is a point of view that orography is not necessary for the blocking occurrence but does support its development (see [144]; and references therein).

With an increase in  $\Delta T$  and a corresponding increase in the available potential energy stored in the main flow, the degree of its baroclinic instability increases. As a consequence, the Lorenz energy cycle of the atmosphere [145] intensifies. This leads to intensification of westerlies and of large-scale jet streams in the atmosphere and, as a reverse reaction, to an increase in the frequency of atmospheric blocking. The latter is Rossby’s [146] famous scenario for the emergence of atmospheric blocking; see also [139]. A key ingredient of Rossby’s theoretical scheme is accounting for the beta-effect. The observed increase in the frequency of blocking

in the winter season compared to the summer season, as well as an increase in the frequency of blocking during global cooling (e.g., [147, 148]), are highly consistent with this scenario.

Meanwhile, the last two decades have demonstrated an increase in blocking frequency accompanying general warming at high-latitudes (Arctic Amplification), the mechanism of which is not entirely clear. A widely accepted paradigm in the climate community is that the shift to a less zonal type of circulation facilitates meridional excursions of air masses and, in particular, provokes blocking action [149]. Various aspects of reproducing future trends in blocking activity by climate models are discussed in [150] and in [151].

Kurgansky [152] attempted to unify the above paradigm with Rossby's ideas using a two-zone atmospheric circulation model over a hemisphere. The surface area of the proportion of extratropical zone occupied by migratory eddies (cyclones and anticyclones) was accepted as a measure of baroclinic instability (baroclinic chaos) over the hemisphere. The principle of maximum of the (informational) entropy of this eddy regime was applied to determine the climate equilibrium latitude of the boundary between the two zones. The model inference was obtained that the area occupied by blocking highs, which is formally included in the extratropical zone but free of eddies, increases with both global cooling (increase in  $\Delta T$ ) and global warming (decrease in  $\Delta T$ ). At the same time, modern conditions (more precisely, the conditions of the end of the 20<sup>th</sup> century) correspond to the minimum of blocking action.

An interesting attempt was made in [153] to reveal the dynamic mechanism explaining the increase in blocking frequency along with a decrease in  $\Delta T$ . These authors proceeded from the fact that, unlike the classical mechanism of baroclinic instability, the decisive role here is played by motions on a planetary scale, the so-called geostrophic motions of the second type [154]. Therefore, the momentum equations reduce to the Sverdrup relation, which describes the balance of the meridional advection of the planetary vorticity and the vertical stretching of the vortex tubes. The subtle point is that in this case the Boussinesq approximation is abandoned and the average (standard) density of the atmosphere is assumed to decrease exponentially with scale height  $H$ . Basically, an anelastic approximation is used. In this case, the Sverdrup relation takes the form

$$\beta v = \frac{\partial w}{\partial z} - \frac{w}{H}. \quad (47)$$

For specific calculations, a two-layer atmospheric model is used. The atmospheric layer under consideration of thickness  $H$  is divided into two sublayers: lower  $0 \leq z \leq H/2$  and upper  $H/2 \leq z \leq H$ . Relation (47) and the buoyancy equation, both differentiated with respect to  $z$ , are written at the levels  $z = H/4, 3H/4$ . The thermal wind equation is used in the differentiated equation (47), and the vertical velocity field is eliminated between the equations obtained. For the parabolic vertical velocity profile

$$w = w_m \frac{z}{H} \left(1 - \frac{z}{H}\right) \quad (48)$$

adopted in the cited work, due to the second term on the right-hand side of (47), the asymmetry necessary for baroclinic instability to occur arises between the equations of the upper and lower layers. According to [153], this instability is possible if the following inequalities are satisfied (in our notation)

$$0 \leq \Delta U \leq \frac{1}{2} \beta L_R^2, \quad (49)$$

where  $\Delta U$  is the velocity shear of the main flow between the upper and lower levels and  $L_R = NH/f_0$  is the Rossby deformation radius. Unlike the classical criterion of baroclinic instability in the two-level Phillips model, here the instability is favored by small values of the vertical velocity shear  $\Delta U$ , that is by small values of  $\Delta T$ , while the beta effect is a destabilizing factor. More details about the problem statement and its solution can be found in the cited work. An interesting question, especially in terms of possible applications to laboratory experiments,

is whether such instability can manifest itself in some baroclinic fluid model, but within the Boussinesq approximation? In other words, to what extent is it necessary to abandon Boussinesq approximation?

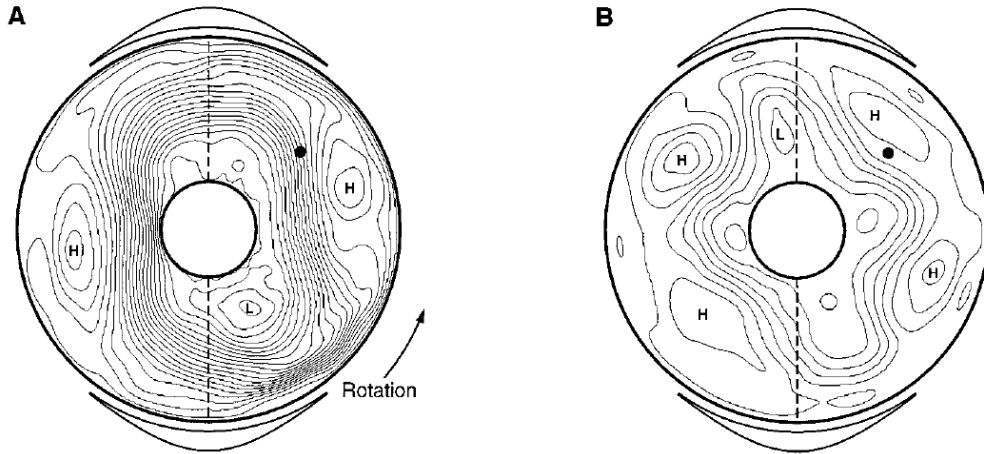


**Figure 9.** Time-averaged stream function contours derived from experimental data for (A) zonal and (B) blocked flow. The Rossby numbers for the zonal and blocked flows are  $0.33 \pm 0.02$  and  $0.22 \pm 0.02$ , respectively. The tops of the ridges are indicated by dashed lines, and the profile of each ridge is shown by black curves outside the rim of the round panels. The black dots indicate the horizontal location of a hot-film probe. Figure has been taken from [155] (with permission).

We have described the state of research into the blocking phenomenon in more detail here because we believe that the baroclinic experiment in conjunction with numerical modelling is well suited to clarifying fundamental processes mentioned above. Most experimental studies on blocking focus on the aspect of flow/topography interactions. Weeks et al. [155] used the barotropic experimental setup by [125] to understand transitions between blocked and zonal flows in an rotating annulus with large-scale topography. An example of a block and a zonal flow situation is displayed in Figure 9. When the flow is blocked a much larger variability of the wave could be observed. Weeks et al. [155] conjectured that the two states correspond to two basins of attraction, connected by a heteroclinic orbit. For the observed multiple equilibria the wave/topography interactions are essential. However, note that even in the absence of topography, switches between different baroclinic regimes have been observed for the flat bottom thermally driven annulus [34] as well as for a two-layer setup using water for the upper and a dilute sugar solution for the bottom layer [156].

More recently, in a series of papers, wave/topography interactions and blocking have been investigated in more detail with the Hide setup of the differentially heated rotating annulus. The authors of [100, 157] and [158] studied topographic resonance and multiple flow regimes. In particular, Marshall and Read [158] found a “stationary-transition” regime where oscillations between a stationary wavenumber-3 flow and axisymmetric or chaotic flows could be found. Wave-zonal-flow and wave-wave interactions (triads) were part of detected nonlinear instabilities. In a follow-up study, the same authors [37] replaced the wavenumber-3 topography by an isolated ridge that partially blocked the flow. Using this configuration, the occurrence of multiple baroclinic flow states have been studied. Again wave triads could be found, this time two triads have been noted sharing a wavenumber-1 mode. Finally, Marshall and Read [159] demonstrated that

blocking can also be induced by a local thermal forcing. Analogies with the atmospheric Walker circulation have been drawn and it was suggested that for the Martian atmosphere it is the thermal forcing that leads to its dominant low-wavenumber flow structures.

The  $\beta$ -effect plays an important role for baroclinic instability and also for the special characteristics of multiple flow regimes. The studies [34, 156, 157], and [100] considered an  $f$ -plane, [37, 125, 155, 158], and [159] used a  $\beta$ -plane, by mounting a sloping bottom or slanted top lid.

As has become clear with the above the occurrence and the frequency of blocking depends on the meridional (radial) temperature gradient. This gradient shows natural fluctuations but also changes due to climate change. Blocking will hence be influenced by these changes [150]. In the following section, findings on changes in the frequency of extreme events from baroclinic wave tank experiments will be discussed.

### 3.6. *Climate and extreme values*

Earth's atmospheric circulation at mid-latitudes and the propagation of Rossby waves is driven by the large-scale meridional gradient of the air temperature. Therefore, as the change of the characteristic "Equator-to-pole" temperature contrast parameter  $\Delta T$  impacts the thermal Rossby number  $Ro_T$ , it may also affect the general character of the flow. In the Earth system  $\Delta T$  exhibits periodic (seasonal) changes through a year, superimposed onto a decreasing trend which has been observed in the weather stations and satellite data throughout the past decades, in parallel with the ongoing global warming. Temperature increase in the Arctic since 1979 has been reported to be more than four times larger than the increase of the global average, a process referred to as Arctic amplification [160].

The decreasing  $Ro_T$  influences the "waviness" of the polar jet stream separating the colder polar domain from the warmer mid-latitudes, as well as the typical extent of its North-to-South detours and the wind speeds in it. The conceptual baroclinic annulus model of the mid-latitude circulation provides a remarkable test bed for investigating Rossby waves in a system whose dynamics are driven by a temperature contrast  $\Delta T$  prescribed by the thermal boundary conditions at the cylindrical sidewalls, and Coriolis force. Experiments in this configuration can help disentangle the complex causal connections of processes which cannot be studied separately in the real Earth system, and provide useful input to the problem of whether or not the wavier jets emerging due to Arctic amplification are also associated with stronger temperature extremes.

A convincing demonstration of the fact that nonlinear statistical features of daily mid-latitude temperature fluctuation time series from the atmospheric boundary layer can generally be reproduced in a rotating annulus experiment was performed by Gyüre et al. in 2007 [161]. Their seminal paper contrasted the time-reversal asymmetry of daily temperature time series from meteorological station data of the Global Daily Climatology Network (GDCN, compiled by the National Climatic Data Center), considering one day temperature differences. They found that the number of subsequent warming steps (i.e. consecutive days where the temperature is higher than on the previous day) is significantly larger than the number of cooling steps in the mid-latitudes, regardless of the length of the investigated records. In other words: large abrupt cooling events are typically followed by slower gradual warming. This strong asymmetry fades away if not consecutive days but larger time differences are compared, as the "memory" (persistence) of weather phenomena is known to have a timescale of a few days, after which the correlation – and the nonlinear, time-asymmetric behavior – vanishes.

In the rotating annulus of the Budapest von Kármán Laboratory (with  $Ro_T = 0.01$ – $0.075$  and  $Ta = 4.47 \cdot 10^9$ – $2.8 \cdot 10^{10}$ , well within the irregular Rossby wave regime) Gyüre et al. implemented analogous measurements with temperature sensors placed in the vicinity of the bottom plate

of the tank, which recorded “daily” temperatures for approx. 5 – 6000 revolutions. In these experiments the same marked asymmetries (with the quantitative agreement of the evaluated time-reversal asymmetry parameters) were observed as in the station data, underlying the physical analogy between the quasi-geostrophic turbulence of the troposphere and the differentially heated rotating annulus.

The above experiment featured constant thermal boundary conditions. In the dynamics of a changing climate a fundamental theoretical problem lies in the very definition of “climate”: the Earth system is a nonstationary one, yet, the empirically obtainable measures of the climate state are time averages of certain observables (e.g., global mean temperature). *Changing* climate implies that on the decadal timescale the “average” behavior itself is also evolving, making the statistical interpretation of the results problematic, mostly in situations where the climate change is abrupt. Theoretically, as introduced by Rameiras et al. [162] for nonlinear systems subject to time-dependent driving and specifically in climatology by Ghil et al. [163], a consistent definition of climatic averages (and other statistics) in such systems could only be achieved via ensemble- (and not time-) averaging. The statistics over a multitude of “parallel histories” has to be considered, each subjected to the very same time-dependent external driving. Then, one can obtain “ensemble statistics” for each time instant  $t$  of the changing climate, a distribution with respect to which, for instance, the extremity of a given measured data point (e.g. daily temperature value) can be evaluated.

Obviously, since only a single realization of the actual Earth system exists, such empirical measures cannot be obtained for the real climate. However, experimental (and numerical) models can be repeated many times under identical pre-defined time-dependent forcing scenarios. Then the comparison of the obtained ensemble statistics with the traditional temporal statistics from a single experiment can teach us important lessons about the nature of such systems.

Results from a climate-change-inspired baroclinic annulus experiment featuring an ensemble of nine experiments with identical time-dependent  $\Delta T(t)$  temperature contrast forcing were reported in [164]. The runs were conducted in the small rotating annulus of the Brandenburg University of Technology (BTU) shown in Figure 3 with parameters  $Ta = 9.18 \cdot 10^8$  and  $Ro_T = 0.013\text{--}0.041$ . From each ensemble member pointwise temperature time series throughout 3300 revolutions (“days”) were evaluated, with the onset of ‘climate change’ occurring exactly at half time: before that  $\Delta T$ , which was then followed by an exponential decay  $\Delta T \sim e^{-t/\tau}$  with  $\tau \approx 360$  revolutions.

In the experiments, traditional single-realization statistics – e.g. standard deviations – and their ensemble-based counterparts were compared. It was found that based on the traditional methods (calculating temporal standard deviations of different time intervals) the change in the characteristic amplitude of the irregular temperature fluctuations was often not detectable, whereas in terms of the ensemble statistics the onset of the  $\Delta T$  decrease clearly resulted in a marked increase of the ensemble standard deviation. This observation implies that a changing climate in a certain sense is more “sensitive” to the small perturbations than a quasi-stationary one, but the size distribution of temperature fluctuations obtained from an individual realization does not necessarily reveal this property. Even in a stationary climate model, however, the effect of the equator-to-pole  $\Delta T$  on the extreme temperatures in the mid-latitude weather is far from being trivial. A series of experimental works conducted in baroclinic annuli were dedicated to explore jet stream variability and the character of temperature distributions as a function of  $\Delta T$ . Rodda et al. [165] performed series of runs in the BTU small annulus (see Figure 3), where various values of (constant)  $\Delta T$  were set, and the temperature statistics were obtained via infrared thermographic imaging of the free water surface. The results confirmed that a smaller  $\Delta T$  yields slower eastward propagation of the jet along the boundary of the Rossby wave, and also indicated that (with decreasing  $\Delta T$ ) the variability of temperatures *decreases* – the histogram



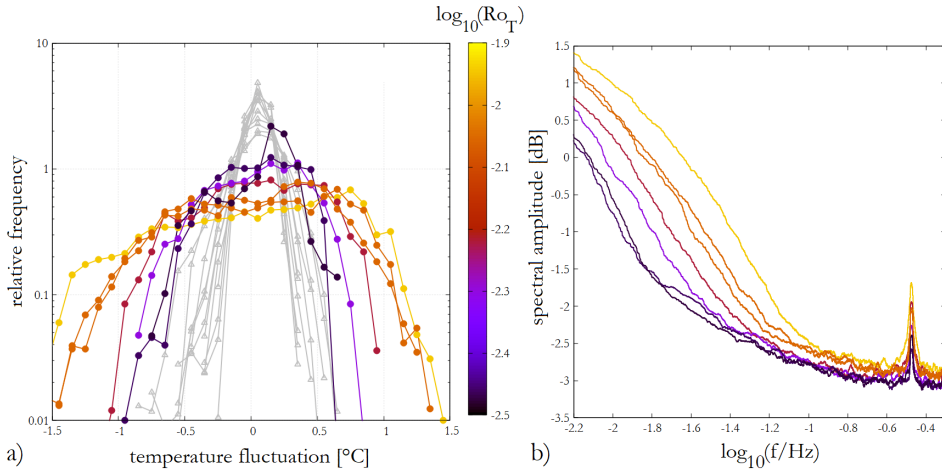


**Figure 10.** Histograms (a) and Fourier spectra (b) of fluctuations in temperature time series from rotating annulus experiments (BTU small tank). The coloring follows the logarithm of the thermal Rossby number  $Ro_T$  for each experiment. Apparently, with decreasing  $Ro_T$  – proportional to temperature contrast  $\Delta T$  – the histograms become narrower, but the “small-slope” spectral domain (indicating less correlated behavior) widens, implying decreasing persistence. Figure taken from [167] (with permission).

of temperature fluctuations becomes narrower – at the “polar” and mid-radius domains of the tank, but *increases* at the “subtropical” region, closer to the outer rim, with decreasing  $\Delta T$ . This finding was also in qualitative agreement with the NCEP reanalysis data based on actual weather station observations. The study showed that extreme events (defined as temperature values out of the 2-StDev interval around the mean) become more frequent if  $\Delta T$  is set lower, even if these extremes are milder.

Similar conclusions were reported recently in the numerical minimal modeling of Rossby waves by Geen et al. [166], and in the experimental work of Vincze et al. [167], where the scaling of the width of the temperature fluctuation histograms, and the spectral properties of the time series were analyzed in a broader range of  $Ro_T$ , combining experiments from the large annulus at the Geophysical Fluid Dynamics Institute (GFDI) of the Florida State University, and the small tank at BTU. The authors found that the width of temperature fluctuation histograms in the vicinity of the bottom of the tank at mid-radius scales linearly with  $Ro_T$ , and also reported that the persistence (correlation timescale) of the “weather” in the tank decreases with  $\Delta T$ , hence in the sense of greater unpredictability, the weather indeed becomes more extreme with the decreased  $\Delta T$ , but this is not associated with the widening of the range of temperature anomalies (Figure 10).

Harlander et al. [168] conducted an extremely long (24-hour) rotating annulus experiment – at fixed stationary values of  $Ro_T$  and  $Ta$  – where “daily” surface temperature fields were analyzed, and the largest spatial mean temperature within each “month” (30-revolution interval) was logged. The so-called shape, scale, and location parameters of the generalized extreme value (GEV) distribution function were fitted to the empirical histogram of these monthly maximum values, and the resulting values were compared to those obtained via an identical procedure from 8-year series of daily atmospheric data. The comparison showed a good agreement, indicating that this laboratory model be a useful tool for investigating extreme event distributions of the climate system.

In the oceanic system, the only region of the planet where a dominantly zonal flow – analogous to the atmospheric jet stream – in the ocean can make a full circle around the globe without getting deflected by a meridional continental boundary is the Southern Ocean, where the strongest near-surface ocean current, the Antarctic Circumpolar Circulation (ACC) is to be found. This current is thought to be largely, but not entirely, wind-driven. The ACC has a particularly important climatic effect: it blocks warm tropical meridional ocean currents from reaching Antarctica, thus helping to maintain the continent’s permanent ice cover. It is known from paleoclimate records that the glaciation of Antarctica happened roughly about the same geological epoch as the opening of the Drake Passage, where earlier the circumpolar flow had been interrupted by a continental bridge connecting the tip of South America and the Antarctic Peninsula. Both events took place at the Eocene-Oligocene transition (EOT) 34 million years ago, but their causal connections are still matter of debate. Bozóki et al. [169], and Vincze et al. [170] performed experiments in baroclinic annuli with the standard configuration, and a closed Drake Passage-like version where the azimuthal flow was blocked with a full-depth radial (“meridional”), thermally insulating wall.

They found that in the “closed” case a persistent azimuthal temperature gradient emerged whose magnitude scales linearly with the “meridional” temperature contrast. Furthermore, seemingly contradicting paleoclimatic data, the presence of the radial barrier yielded lower values of the surface temperature in the tank than those in the “open” experiments. This difference can be explained by the importance of the role ice-albedo feedback plays in an EOT-like transition, an aspect that is not captured in the laboratory setting. This idea was confirmed by numerical simulations conducted in a numerical global climate model, where the comparison of “closed” and “open” configurations could be made both with and without sea ice feedback. These runs indeed yielded opposite effects on sea-surface temperature and are therefore consistent with both the laboratory experiment and the paleoclimate data.

### 3.7. *Internal waves and small-scale instabilities*

At least for shallow atmospheres like the one of the Earth, the aspect ratio  $\Gamma_d = d/L$  of the experiment is too large for parameter similarity. As long as  $Bu$  is small enough, this does not have a fundamental effect for the large-scale dynamics under consideration. On the other hand, it is a problem when the generation of small-scale waves is considered. The differentially heated rotating annulus is a stratified rotating fluid that not only supports long Eady and Rossby waves but also short inertia-gravity waves (IGWs). For strongly (weakly) stratified rotating fluids such waves occur in the frequency band  $f < \omega < N$  ( $N < \omega < f$ ). The atmosphere of the Earth and the upper ocean are strongly stratified ( $N/f \approx 10^2$ ) (whereas the deep ocean is weakly stratified only). It is therefore of interest to look for the occurrence of IGWs in the baroclinic wave tank.

#### 3.7.1. *Boundary layer instabilities*

In the atmosphere, there are different main source mechanisms for IGWs: flow over mountains, convection, and jets and fronts [84]. For the baroclinic wave experiment, there is another source and this is boundary layer instability. Jacoby et al. [171] observed short period waves in the vicinity of the inner cooled cylinder of their differentially heated rotating annulus experiment and corresponding numerical simulations. Analysing their data they were able to prove that the waves fall nicely into the inertia-gravity wave band. Using the dispersion relation

$$\omega = \left( \frac{f^2 m^2 + N^2 (k^2 + l^2)}{k^2 + l^2 + m^2} \right)^{1/2} + Uk, \quad (50)$$

with  $f = 2\Omega$  the Coriolis parameter,  $N$  the buoyancy frequency,  $U$  the azimuthal mean flow, and  $(k, l, m)$  the wave vector, one finds from their experiment with  $f = 4.06$  rad/s,  $N = 0.5$  rad/s,

$U = 0.066$  mm/s and a wave vector  $(k, l, m) = (2\pi/0.1, 2\pi/0.2, 2\pi/1.1)$  cm<sup>-1</sup> an intrinsic frequency of  $\omega = 1.01$  rad/s. We see that, in contrast to atmospheric conditions, the experiment in [171] was in the weakly stratified regime with  $N < \omega < f$ . As we will see later, this situation is rather typical for baroclinic wave experiments with an aspect ratio (comparing fluid depth,  $d$ , and gap width,  $L$ ) of order one.

To explain the excitation of these waves, Jacoby et al. [171] applied the convective boundary layer model from [172]. In this model a viscous fluid with kinematic viscosity  $\nu$  is bounded by an infinite vertical wall. The wall has a constant vertical temperature gradient. Moreover, between the wall and the fluid there is a fixed horizontal temperature difference with respect to the fluid far in the interior. Along the wall, a thermal boundary layer of constant thickness  $\delta_B$  is considered in which the amplitude of the vertical velocity  $W$  is large. Gill and Davey [172] plotted  $Pr^{1/2}Re$  against the vertical wave number where  $Pr$  is the Prandtl and  $Re = \sqrt{2}W\delta_B/\nu$  is the Reynolds number. Numerically, Jacoby et al. [171] found that for their experimental parameters the critical Reynolds number is exceeded in the boundary layer of the cooled inner vertical wall of the annulus.

Based on direct numerical simulations with high-resolution pseudospectral methods a detailed study on small-scale instabilities occurring in a baroclinic cavity has been carried out [173]. In an experiment with a Prandtl number of 16 and  $\Omega = 0.5125$  rad/s these authors observed small-scale fluctuations connected to baroclinic waves. These small-scale fluctuations occur for vacillating baroclinic waves studied with  $\Omega = 0.5125$  rad/s, but also for steady baroclinic waves that could be found for smaller  $\Omega$ . Using similar arguments as given in [171] they showed that the fluctuations correspond with inertia-gravity waves, occurring again in the regime of small frequency ratio  $N/f = 0.17$ . In contrast to [171], the authors emphasized that the IGWs are attached to the baroclinic waves and they develop a somewhat more sophisticated theory beyond the model by [172] that does not include rotational effects. However, the inner cold wall of the annulus plays an important role in [173], too. The latter authors showed that the small-scale fluctuations propagate vertically along the inner cold wall over three “ridges” following their baroclinic wave-3 flow. Towards the upper part of the cavity the characteristics of the IGWs developed to almost inertial waves with vertical propagation only. This latter feature might be due to the fact that in the whole cavity  $N < f$  with a particular small  $N$  in the upper region of the annulus.

According to [173], the instability in the lower part of the downward flow along the inner wall is ultimately caused by Kelvin-Helmholtz instability. These authors find numerically that the local Richardson number,  $Ri = N^2/U_z^2$ , falls below the critical value of 1/4, signaling shear instability. This instability invokes resonant over-reflection, that is, a density overturn was observed close to the inner wall along the bottom boundary layer, associated with the presence of a reversal flow and a stagnation point. The scenario described is strongly reminiscent of the one which has already been described by [174]. It should be noted that critical  $Ri$  values cannot be found everywhere along the inner edge but only where the cold baroclinic vortices are in contact with the inner wall. Therefore, the instability exciting IGWs is intimately linked to the large-scale baroclinic wave field.

In a further study, von Larcher et al. [43] took a close look on the small-scale features at the cooled inner and heated outer wall by using two different numerical models and experimental data. In Figure 11 isosurface snapshots of the small-scale instabilities in the vertical sidewall regions are displayed. It could be shown that only the structures at the inner wall (Figure 11 (a)) correspond to IGWs able to radiate into the bulk of the baroclinic cavity. In contrast, the ripples at the outer wall (Figure 11 (b)) are not IGWs and they are due to inertial instability rather than the thermal boundary layer instability. These features remain trapped to the boundary layer of the outer wall and cannot propagate inward, in contrast to the IGWs generated at the inner wall that propagate outward.

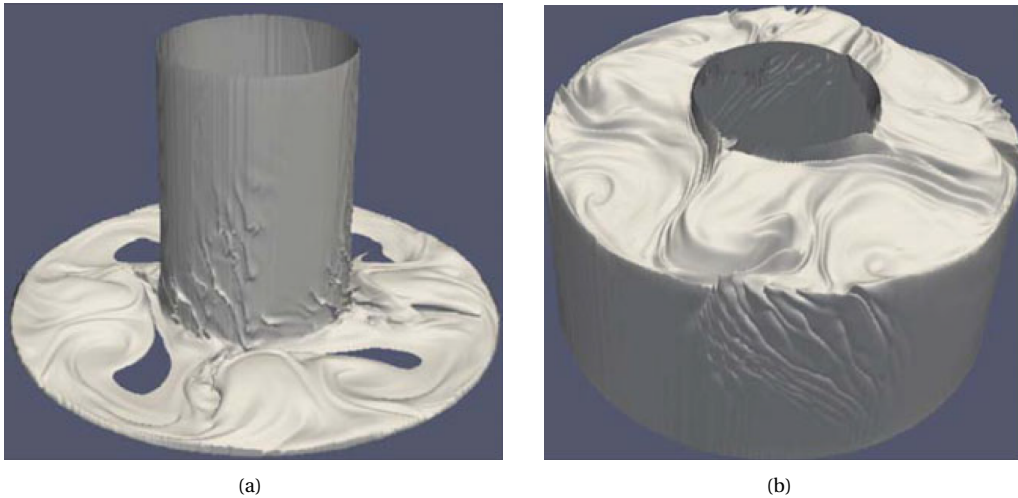


**Figure 11.** Isosurface snapshots of the small-scale instabilities in the vertical sidewall regions simulated with the EULAG model. a)  $T = 296.15$  K, and b)  $T = 291.15$  K. It should be noted that the holes in a) are due to the fact that the specific value of the isosurface is not given there at the time increment shown. Figure from [43] (with permission).

A necessary condition for inertial instability in an ideal fluid was discovered by [175], taking into account the general rotation of the fluid, it reads  $d(U(r)r + \Omega r^2)^2/dr \leq 0$ , where  $U(r)$  is the azimuthal flow. For the differentially heated rotating annulus this criterion is insufficient since there is not only an azimuthal velocity but also a vertical velocity,  $W$ , at the outer wall. The criterion found by Hart and Kittelman [176] is more appropriate and it reads

$$2\Omega \cos \gamma \left( 2\Omega \cos \gamma + \frac{d|\tilde{U}|}{dr} \right) < 0, \quad (51)$$

where  $\tilde{U}$  is the velocity tangent to the wall at angle  $\gamma$  with  $\tan \gamma = W/U$ . This criterion is fulfilled in regions where the ripples in the outer boundary layer can be found. However, stratification has been neglected in the stability criterion (51).

### 3.7.2. Imbalance

It is compelling to use the differentially heated rotating annulus to study another IGW generation mechanism, spontaneous imbalance at baroclinic jets and fronts, which is an important source for the occurrence of IGWs in the atmosphere [177]. For the large-scale atmospheric flows, Froude number,  $Fr = U/NH$ , (also the centrifugal Froude number  $Fr_c = \Omega^2 L/g$ ), Rossby number  $Ro = U/2\Omega L$ , and the aspect ratio  $H/L$  are much smaller than one. To reach similarity between the experiment and natural flows, these nondimensional parameters need to be small in the experiment as well. Using a suitable differential heating and rotation this is possible; however, compared to the atmosphere, the aspect ratio is typically too large in the experiment.

This situation is of particular relevance here, because the aspect ratio determines not only the instability of the baroclinic waves but also the special characteristics of IGWs. Put simply, keeping the radial temperature difference  $\Delta T$  constant but reducing the depth  $H$  leads to larger  $N$ . The reason is that the temperature difference between the inner and outer wall also determines the difference between the surface and the bottom. This implies that for the standard setup of the baroclinic wave tank with  $H/L \approx 1$ , the ratio  $N/f < 1$  and not  $\sim 10^2$  like in the atmosphere. In

contrast to the atmosphere, small-scale IGWs will be strongly affected by rotation (see [178, 179] for more details).

The importance of the aspect and frequency ratio for baroclinic instability can be seen from the Burger number given in equation (6) where  $L = b - a$  is the annulus' gap width and  $d$  the annulus' fluid depth. For baroclinic instability, according to [5], a critical value of  $Bu$  depends on the horizontal wave numbers. For experiments with the baroclinic cavity we usually see a radial wave number of one (i.e. a structure  $\sim \sin \pi y$ ,  $0 \leq y \leq 1$ , where  $y$  is the radial direction). For baroclinic instability,  $Bu$  needs to be smaller than  $0.58/(1 + k^2/\pi^2)$  where  $k$  is the azimuthal wave number. Hide and Mason [34] found that for baroclinic wave experiments the azimuthal wave number depends on the geometry of the annulus,

$$\frac{\pi (b + a)}{4 (b - a)} \leq k \leq \frac{3\pi (b + a)}{4 (b - a)}. \quad (52)$$

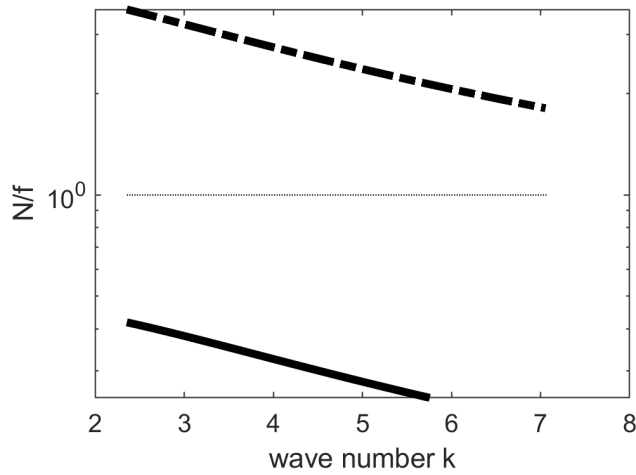


**Figure 12.** The critical ratio  $N/f$  in logarithmic scale over the wave number  $k$  for the small BTU tank ( $d/L = 1.60$ , solid line) and the large BTU tank ( $d/L = 0.17$ , dashed-dotted line).  $N/f = 1$  is shown by the thin dotted line. The figure should be compared with [178, Figures 3c and 5c].

Figure 12 shows the wave number range and  $N/f$  at the critical value for  $Bu$  for the small  $((a, b) = (4.5, 12)\text{cm})$  and the large  $((a, b) = (30.0, 70.0)\text{cm})$  baroclinic cavity at the Brandenburg University of Technology (BTU). Obviously, the frequency ratio is larger (smaller) than 1 for the large (small) tank experiments. Therefore, for conducting IGW-related experiments with regard to atmospheric conditions, experimental setups with a small aspect ratio are more suitable.

To our knowledge, the first systematic study of the interaction between the large-scale nearly balanced flow and ageostrophic IGWs in a baroclinic wave tank was done by Lovegrove et al. [29]. These authors used a two layer setup with two immiscible fluids of different density, and baroclinic instability was not due to differential heating but a mechanical forcing. The upper lid of the experiment rotated slightly faster than the bottom driving the necessary vertical shear in the horizontal velocity. The aim was to find interactions between the balanced baroclinic waves that have basically no horizontal divergence, and the unbalanced or ageostrophic IGWs. Verified via (50), IGWs were found in flow regimes with amplitude vacillations and they were located mainly along the baroclinic fronts. Since the waves could be found during certain phases of the amplitude vacillation cycle, Lovegrove et al. [29] assumed that imbalance of the large-scale flow

generates the IGWs. This work was continued by [180] and they could show that for parameters that determine a baroclinic wave transition region, the IGWs play a role in terms of azimuthal wave number selection.

Somewhat later, Williams et al. [30] investigated the source mechanism for the IGW wave generation in more detail. The two possible mechanisms considered were spontaneous adjustment of the large-scale flow, and Kelvin–Helmholtz shear instability. The authors found that for stable baroclinic waves, the small scale waves can be found only for subcritical bulk two-layer Richardson numbers, defined as  $Ri = 2g'\delta_E/r^2\Delta\Omega^2$ , where  $g'$  is reduced gravity,  $\delta_E = (\nu/\Omega)^{1/2}$  is the upper/lower Ekman layer thickness,  $\nu$  kinematic viscosity, and  $r$  the radius. For unstable baroclinic waves, they found agreement between the spatial locations of IGW emission and regions in which the model Lighthill/Ford IGW source term is large, implying that the short waves in the baroclinically unstable case are freely propagating IGWs generated by spontaneous adjustment of the large-scale flow [181].

In a later work Williams et al. [182] confirmed the existence of spontaneous emission in their experiment, which implied an inevitable emission of IGWs for Rossby numbers of the same order as in the ocean and the atmosphere. They speculated that the emission of IGWs by mesoscale eddies may be a relevant process providing energy for mixing in the deep ocean. However, Flór et al. [183] questioned spontaneous emission as the dominant source mechanism for the experimentally observed IGWs. With their own experiments, they proposed that a special shear instability called *Hölmboë instability* is responsible for the IGWs. Note that this instability occurs in a two-layer fluid with a sharp interface by a resonance between an IGW and a wavelike background disturbance where the background shear varies vertically. Flór et al. [183] argued that for the generation of IGW radiation in a two-layer baroclinic cavity, Hölmboë instability could also be a candidate in addition to spontaneous emission.

For a closer connection to atmospheric conditions, Borchert et al. [178] did numerical simulations for a classical differentially heated rotating annulus with a heated outer and a cooled inner wall. For such a setup, a continuous thermal stratification develops. They considered two different geometries, similar to the two baroclinic wave experiments available at the BTU lab (see Figure 12). In their simulations they found IGWs generated at the inner vertical boundary layer as in [171] as well as at the frontal zone of the baroclinic waves. The latter have been attributed to spontaneous emission, however, these IGWs look very different from the one shown by [29]. That the patterns actually correspond to IGWs has been tested by a modal decomposition, based on linear IGW theory. In the solutions by [178] the scale-separation between the IGWs and the baroclinic waves was not so clear as in [29]. However, the IGWs in the large and small annulus configurations resemble, in their spatial structure, those observed in simulations of an idealized life cycle of an unstable baroclinic wave in the atmosphere (see e.g. [184]).

The numerical findings by [178] have been studied experimentally by [179] and [107]. The first evidence of IGWs in the continuously stratified annulus was reported but it became clear, that in spite of a good agreement with respect to the baroclinic waves, the experimentally derived buoyancy frequency  $N$  deviated from the one found numerically. The largest values of  $N$  occurred along the baroclinic jet axis and, in contrast to the numerical data, the IGWs in the experiment seemed to be trapped in the jet region.

Using data from the large BTU annulus configuration (see Figure 12), following [185] and separating the spectra into vortex and a wave components, Rodda and Harlander [107] could reproduce atmospheric spectra showing a  $-3$  slope for the baroclinic waves but a  $-5/3$  slope for the “meso-scale” part in which the IGWs occur. By computing the ratio between the divergent and the rotational component of the kinetic energy and checking the local Rossby number  $Ro_l = |\zeta_z|/f$ , where  $\zeta_z$  is the vertical vorticity and  $f$  is the Coriolis parameter, [107] concluded that linear IGWs are responsible for the shallow part of the spectrum. This conclusion was drawn

from the fact that the energy ratio was larger than one in regions where  $Ro_l < 1$  [186].

We mention finally baroclinic wave tank experiments that deviate from the classical setup by adding a continuous salt stratification to the thermal stratification [187]. The reason for this setup was a better control of the  $N/f$  ratio. The experiments were done with a small tank setup and, as we discussed above, this usually implies a small frequency ratio. However, adding a linear salt stratification gives additional freedom in adjusting  $N/f$ . This experiment was, in fact, the first to prove the existence of IGWs on fronts for a case with continuous stratification.

### 3.7.3. Topography

Remarkably, the best investigated IGW source in the atmosphere is not well studied in the context of baroclinic tank experiments. Interactions between topography and baroclinic waves of similar length scales have been studied mainly with regard to blocking (see Section 3.5). On the other hand there is a large literature on channel experiments on IGW generation by topography and the wave radiation into the flow (for a review see e.g. [188]). However, for the classical baroclinic cavity setup, for which the zonal flow is determined by the thermal wind relation (4), experiments have been conducted with topography having a characteristic length larger than the Rossby deformation radius,  $L_R = (U_T(b-a)/(\Omega))^{1/2}$  and the focus was on the interaction between topography and planetary Rossby waves.

Recently, however, Stewart et al. [9] modified the setup by differentially rotating a small-scale topography with respect to the tank (and also to  $U_T$ ). In this case, the experiments are closer to the IGW experiments reviewed in [188] and the interaction between the topographically excited IGWs with baroclinic eddies could be studied. For the excitation of IGWs, the topographic Froude number  $Fr_B = U/Nh_B$ , with  $h_B$  the height of the topography, should be one or larger. This can be reached by using the mentioned differentially moving ridge. (Note that Stewart et al. [9] defined a lee wave Froude number as  $Fr_B^{-1}$ .) The authors found that standing features, in particular upstream internal bores play an important role for steering the flow. Such features occurred over a wide range of flow speeds but only when the internal Froude number,  $Fr_i = n\pi Fr$ , where  $n$  is the vertical mode number, is smaller than one.

### 3.7.4. Convection

Convection can trigger IGWs in the atmosphere e.g. when deep convection deforms the tropopause which in turn emits IGWs into the strongly stratified stratosphere [84]. Such processes have been studied experimentally and we just give two recent references for an overview, [189] and [190]. In the context of baroclinic wave experiments this has, with one exception, not been investigated. Recently, Abide et al. [191] studied numerically surface effects in a large free-surface differentially heated rotating annulus. Knowing that small aspect ratio setups are more suitable for generating atmosphere-like IGWs, one must on the other hand take into account that there is a significant heat exchange at the free surface. It was found in [191] that the onset of baroclinic instability can be suppressed if the ambient temperature is higher than the mean temperature at the surface. Moreover, if the temperature of the environment is lower than the surface mean temperature, small-scale IGW-like features can be seen at the surface which are almost certainly caused by convective instability. These findings have not been confirmed experimentally. In the experiments, evaporation and the corresponding cooling can also affect the stability of the surface layer.

To round off the section, we can finally ask what role IGWs might play for the transition from the regular baroclinic wave regime to geostrophic turbulence. Using direct numerical simulation to investigate the flow in an air-filled baroclinic cavity, Read et al. [42] showed that small-scale fluctuations gradually break the regularity of the baroclinic waves, leading to structural wave vacillations before the transition to geostrophic turbulence. However, for an air-filled annulus with Prandtl numbers smaller than one, the small-scale features did not correspond with IGWs. Later, Randriamampianina and Crespo del Arco [173] speculated that IGW generation and not only small-scale fluctuations might be a relevant process for the transition. However, to our knowledge, this question on the role of IGWs for the transition process could not be conclusively answered yet.

### 3.8. *Benchmarks*

Experimental minimal models provide superb test-beds for the fine-tuning and validation of complex circulation models of the ocean and the atmosphere. Systematic tests of numerical codes operational in weather forecasting are especially hard to perform, as it is challenging to separate the inaccuracies arising from erroneous numerical implementation and those originating from our incomplete understanding of the processes of Earth's weather system. In the laboratory-based systems, however, all governing equations and boundary conditions are fairly well known and can be adjusted or controlled. Hence, if one uses the weather forecasting codes and numerical methods to simulate the experiment's model flow, the discrepancies cannot be blamed on the complexity of climate, but must be attributed to improper implementation.

In the framework of the MetStröm collaboration (2008–2014) the rotating annulus served as a reference experiment and the model flow was simulated by five different working groups and GCMs, using various numerical approaches, solvers and subgrid-scale parametrization methods [192].

The regular-type Rossby waves on the free water surface of the BTU small annulus have been analyzed in benchmark experiments covering a wide range of rotation rates (and fixed  $\Delta T$ ), also applying different initial conditions (spin-up and spin-down). Five groups of the collaboration have conducted numerical simulations in the same parameter regime using different approaches and solvers trying to reproduce the laboratory results. The experimentally and numerically obtained baroclinic wave patterns have then been contrasted in terms of various parameters, most notably their dominant wave numbers and drift rates. The study found that although most of the numerical codes were rather successful in predicting the waveform of the Rossby waves, almost all of them consistently underestimated their drift rates.

A similar approach – testing operational weather forecasting methods in the rotating annulus – has been followed by Young and Read [193]. They built a forecasting system for the annulus based on the same principles and techniques which are regularly applied by the British MetOffice for atmospheric predictions. Their results showed that a range of flow regimes could be accurately predicted, and forecasts in the regular wave flow regime performed well. Forecasts in the amplitude and structural vacillation flow regimes, however were found to be less accurate in terms of predicting wave drift rates and wavenumber transitions.

## 4. **Conclusions**

In the struggle to understand the atmospheric general circulation [145, 194], the differentially heated rotating annulus has certainly made a contribution in spite of the fact that boundary layers have a more significant effect on the flow in the annulus compared to the flow of Earth's atmosphere. It is also true that laboratory analogues such as the thermally driven rotating annuli



are not exact experimental simulation models, however, they do contain important elements of a complex dynamics that enable a deeper understanding of fundamental aspects and relationships and are hence fully complementary to numerical simulations. The same could be said for the other two basic experiments used also in the context of geophysical flows: the Rayleigh–Bénard (RB) and the Taylor–Couette (TC) experiment. In a sense, the Hide–Fultz experiment reviewed here, combines RB-convection and TC-shear and adds (background) rotation and is hence, with a view on geophysical fluid dynamics, the most “complete” of the trio.

Last year, the Royal Society celebrated the 100 year anniversary of Taylor’s fundamental 1923 paper [195] by a two volume special issue [196, 197]. It is quite a remarkable coincidence that in the same year, Exner [198] did the first experiments on baroclinic instability. More precisely, he operated his experiment in a baroclinically unstable irregular regime where other experimenters before him considered the stable azimuthal regime only [199]. Although of course Taylor’s work had a far greater impact on the development of fluid mechanics than Exner’s article, we can humbly celebrate the 100 year anniversary of the first Hide-Fultz-type experiment with baroclinic instability with this review.

Environmental flows remain challenging [200] and the thermally driven rotating annulus will continue to play a role in the development of theories for convective rotating flows and further as a reference experiment to test numerical models and parameterizations. Numerical models have certainly developed to a level of greater performance, but direct numerical simulations are hardly possible, especially for the large experiments shown in Figure 3. The larger experiments have a free surface and surface effects like surface heat flux or evaporation become more important. These additional boundary conditions make numerical calculations even more time consuming. However, over the last years codes that allow for massively parallel computations have been developed for rotating stratified fluids [201]. Recently one such code was applied to stratified Taylor-Couette flows [202] and it seems possible in the near future to do direct numerical simulations also for large experimental setups. Finally, we note that even for smaller tanks, long simulations, which are necessary, e.g. to answer questions about extreme values, can currently be done only with great effort.

We pointed out that apart from baroclinic instability other types of instability generating small-scale inertia gravity waves are also an inherent part of the annulus fluid dynamics. In the atmosphere, such waves play a fundamental role for the large-scale atmospheric circulation [84]. Hence it is certainly a future task to understand better the interactions of these very different flow scales in the annulus and to uncover the role that the small-scale waves play for the transition to turbulence. Also, nonmodal instability might be worth considering in this context and first attempts have been made to estimate such modes from annulus data [203, 204]. An extensive review on nonmodal instability can be found in [205]. Transient growth is possible only when the linearized Navier-Stokes operator is non-normal and this is usually the case in shear flows. At this point it seems appropriate to refer again to the remarkable similarity in the mathematics of barotropic (shear) and baroclinic instability [194].

Additionally, as pointed out by [206] and recently cited by [9], “modern technologies and analysis techniques have spawned a renaissance in laboratory experiments as these new approaches can provide new insights into processes, like rotating stratified turbulence, that remain challenging and/or infeasible to explore via numerical simulations.” Two of the modern technologies we would like to mention here. One is combining laser induced fluorescence (LIF) with particle image velocimetry (PIV). Caudwell et al. [207] have shown that this technique is well suited for convective flows with a reasonable accuracy of  $0.2^\circ\text{C}$  with respect to temperature. A simultaneous measurement of the velocity field allows for a calculation of key parameters like the Richardson number or the heat flux in the interior of the fluid. LIF used a temperature sensitive dye like Rhodamine B. When this substance is excited with a green laser (532 nm), it emits light in the range

from 565 nm to 585 nm, depending on the temperature of the Rhodamine particles. Since PIV works with light sources of, for example, 532 nm, a wavelength outside the sensitivity of Rhodamine, these two methods can be used simultaneously if suitable filters are used.

The other method we wish to mention is 3D Lagrangian particle tracking [208]. This method allows for the detection of the position, speed, and acceleration of particles in 3D and gives hence a 3D view on a large number of particle tracks. Apart from the attempts described in Section 3.4, the 3D structure of the flow in the baroclinic annulus has not been studied. Many problems related to transport and mixing in geophysical flows are still open and could be attacked by particle tracking. Also, diagnostic tools that have been developed (see, e.g. [209]) to predict the spreading of pollutants could be used in annulus experiments together with 3D particle tracking. As described above for PIV, particle tracking could be combined with LIF to obtain the temperature along particle tracks. Of course, another condition is that all of these experimental techniques need a good optical access to the fluid chamber.

## Acknowledgements

We thank Kial D. Stewart and C. J. Shakespeare for providing updated versions of Figures 1 and 3. U.H. thanks L.R.M. Maas and P. Szabo for helpful discussions and R. Stöbel, S. Rohark, and S. Misera for constant support in the laboratory. M.V. thanks T. Tel, M. Herein, and Z. Trocsanyi for the fruitful discussions. K.S. thanks J. Marshall and J. Whitehead for conversations concerning some of the historical context.

U. Harlander thanks DFG for financial support (HA 2932/8-1&2, HA 2932/17-4), DAAD for funding a series of french-german exchange projects within PROCOPE, and the BTU Graduate Research School (BTU-GRS) for constant support. M.V. Kurgansky was partly supported by funding from the State Assignment (No. FMWR-2022-0011) “Fundamental research into the dynamics of vortex structures and turbulence in geophysical flows”. K. Speer acknowledges the support of NSF Office of Polar Programs (OPP 1643679, OPP 1644172, and OPP 2148517) and Ocean Science (OCE 1658479).

## Declaration of interests

The authors do not work for, advise, own shares in, or receive funds from any organization that could benefit from this article, and have declared no affiliations other than their research organizations.

## References

- [1] D. Fultz, “Experimental analogies to atmospheric motions”, in *Compendium of meteorology* (T. F. Malone, ed.), American Meteorological Society, Boston, MA, 1951, pp. 1235–1248.
- [2] D. Fultz, “A preliminary report on experiments with thermally reproduced lateral mixing in a rotating hemispherical shell of liquid”, *J. Atmos. Sci.* **6** (1949), pp. 17–33.
- [3] M. Ghil, P. L. Read and L. Smith, “Geophysical flows as dynamical systems: the influence of Hide’s experiments”, *Astron. Geophys.* **51** (2010), no. 4, pp. 4.28–4.35.
- [4] J. G. Charney, “The dynamics of long waves in a baroclinic westerly current”, *J. Atmos. Sci.* **4** (1947), pp. 136–162.
- [5] E. T. Eady, “Long waves and cyclone waves”, *Tellus* **1** (1949), no. 3, pp. 33–52.
- [6] V. P. Starr, “Commentaries Concerning Research on the General Circulation”, *Tellus* **6** (1954), no. 3, pp. 268–272.
- [7] R. Hide and P. J. Mason, “Baroclinic waves in a rotating fluid subject to internal heating”, *Philos. Trans. R. Soc. Lond., Ser. A* **268** (1970), no. 1186, pp. 201–232.
- [8] P. R. Gent and H. Leach, “Baroclinic instability in an eccentric annulus”, *J. Fluid Mech.* **77** (1976), no. 4, pp. 769–788.

- [9] K. D. Stewart and C. J. Shakespeare, “On stratified flow over a topographic ridge in a rotating annulus”, *Geophys. Astrophys. Fluid Dyn.* **118** (2024), no. 1, pp. 25–70.
- [10] R. L. Pfeffer and W. W. Fowles, “Wave Dispersion in a Rotating, Differentially Heated Cylindrical Annulus of Fluid”, *J. Atmos. Sci.* **25** (1968), no. 3, pp. 361–371.
- [11] U. Harlander, T. von Larcher, Y. Wang and C. Egbers, “PIV- and LDV-measurements of baroclinic wave interactions in a thermally driven rotating annulus”, *Exp. Fluids* **51** (2011), pp. 37–49.
- [12] G. Buzyna, R. L. Pfeffer and R. Kung, “Kinematic Properties of Wave Amplitude Vacillation in a Thermally Driven Rotating Fluid”, *J. Atmos. Sci.* **46** (1989), no. 17, pp. 2716–2730.
- [13] G.-Q. Li, R. Kung and R. L. Pfeffer, “An Experimental Study of Baroclinic Flows with and without Two-Wave Bottom Topography”, *J. Atmos. Sci.* **43** (1986), no. 22, pp. 2585–2599.
- [14] G. Buzyna, R. L. Pfeffer and R. Kung, “Transition to geostrophic turbulence in a rotating differentially heated annulus of fluid”, *J. Fluid Mech.* **145** (1984), pp. 377–403.
- [15] R. L. Pfeffer, S. Applequist, R. Kung, et al., “Progress in Characterizing the Route to Geostrophic Turbulence and Redesigning Thermally Driven Rotating Annulus Experiments”, *Theor. Comput. Fluid Dyn.* **9** (1997), pp. 253–267.
- [16] W.-G. Früh and P. L. Read, “Wave interactions and the transition to chaos of baroclinic waves in a thermally driven rotating annulus”, *Philos. Trans. R. Soc. Lond., Ser. A* **355** (1997), no. 1722, pp. 101–153.
- [17] R. L. Pfeffer, G. Buzyna and W. W. Fowles, “Synoptic Features and Energetics of Wave-Amplitude Vacillation in a Rotating, Differentially-Heated Fluid”, *J. Atmos. Sci.* **31** (1974), no. 3, pp. 622–645.
- [18] W.-G. Früh, “Amplitude vacillation in baroclinic flows”, in *Modelling Atmospheric and Oceanic Flows: Insights from Laboratory Experiments and Numerical Simulations* (T. von Larcher and P. D. Williams, eds.), American Geophysical Union, 2014, pp. 61–81.
- [19] J. E. Price and H. T. Rossby, “Observations of a barotropic planetary wave in the western North Atlantic”, *J. Mar. Res.* **40** (1982), pp. 543–558.
- [20] P. L. Read, “From mixing to geostrophy: Geostrophic turbulence in atmospheres, oceans and the laboratory”, in *Marine Turbulence: Theories, Observations, and Models* (H. Z. Baumert, J. Simpson and J. Sündermann, eds.), Cambridge University Press, 2005, pp. 406–422.
- [21] P. M. Saunders, “The Instability of a Baroclinic Vortex”, *J. Phys. Oceanogr.* **3** (1973), no. 1, pp. 61–65.
- [22] T. Maxworthy and S. Narimousa, “Unsteady, Turbulent Convection into a Homogeneous, Rotating Fluid, with Oceanographic Applications”, *J. Phys. Oceanogr.* **24** (1994), no. 5, pp. 865–887.
- [23] J. Marshall and F. Schott, “Open-ocean convection: Observations, theory, and models”, *Rev. Geophys.* **37** (1999), no. 1, pp. 1–64.
- [24] P. L. Read, “Transition To Geostrophic Turbulence In The Laboratory, And As A Paradigm In Atmospheres And Oceans”, *Surv. Geophys.* **22** (2001), pp. 265–317.
- [25] P. L. Read, E. P. Pérez, I. M. Moroz and R. M. B. Young, “General circulation of planetary atmospheres: Insights from rotating annulus and related experiments”, in *Modelling Atmospheric and Oceanic Flows: Insights from Laboratory Experiments and Numerical Simulations* (T. v. Larcher and P. D. Williams, eds.), American Geophysical Union, 2014, pp. 9–44.
- [26] P. L. Read, “Dynamics and circulation regimes of terrestrial planets”, *Planet. Space Sci.* **59** (2011), pp. 900–914.
- [27] P. Read, D. Kennedy, N. Lewis, et al., “Baroclinic and barotropic instabilities in planetary atmospheres: energetics, equilibration and adjustment”, *Nonlinear Process. Geophys.* **27** (2020), no. 2, pp. 147–173.
- [28] J. E. Hart, “A Laboratory Study of Baroclinic Instability”, *Geophys. Fluid Dyn.* **3** (1972), pp. 181–209.
- [29] A. F. Lovegrove, P. L. Read and C. J. Richards, “Generation of inertia-gravity waves in a baroclinically unstable fluid”, *Q. J. R. Meteorol. Soc.* **126** (2000), no. 570, pp. 3233–3254.
- [30] P. D. Williams, T. W. N. Haine and P. L. Read, “On the generation mechanisms of short-scale unbalanced modes in rotating two-layer flows with vertical shear”, *J. Fluid Mech.* **528** (2005), pp. 1–22.
- [31] U. Harlander, A. Sukhanovskii, S. Abide, et al., “New Laboratory Experiments to Study the Large-Scale Circulation and Climate Dynamics”, *Atmosphere* **14** (2023), article no. 836.
- [32] R. Hide and W. W. Fowles, “Thermal convection in a rotating annulus of liquid: effect of viscosity on the transition between axisymmetric and non-axisymmetric flow regimes”, *J. Atmos. Sci.* **22** (1965), pp. 541–558.
- [33] J. S. Fein and R. L. Pfeffer, “An experimental study of the effects of Prandtl number on thermal convection in a rotating, differentially heated cylindrical annulus of fluid”, *J. Fluid Mech.* **75** (1976), no. 1, pp. 81–112.
- [34] R. Hide and P. J. Mason, “Sloping convection in a rotating fluid”, *Adv. Phys.* **24** (1975), no. 1, pp. 47–100.
- [35] R. Hide and R. Stoneley, “An experimental study of thermal convection in a rotating liquid”, *Philos. Trans. R. Soc. Lond., Ser. A* **250** (1958), no. 983, pp. 441–478.
- [36] C. A. Smith, K. G. Speer and R. W. Griffiths, “Multiple Zonal Jets in a Differentially Heated Rotating Annulus”, *J. Phys. Oceanogr.* **44** (2014), no. 9, pp. 2273–2291.
- [37] S. D. Marshall and P. L. Read, “An experimental investigation of blocking by partial barriers in a rotating baroclinic annulus”, *Geophys. Astrophys. Fluid Dyn.* **112** (2018), no. 2, pp. 97–129.

- [38] U. Harlander, J. Wenzel, K. Alexandrov, Y. Y. Wang and C. Egbers, “Simultaneous PIV and thermography measurements of partially blocked flow in a differentially heated rotating annulus”, *Exp. Fluids* **52** (2012), pp. 1077–1087.
- [39] H. Scolan and P. L. Read, “A rotating annulus driven by localized convective forcing: a new atmosphere-like experiment”, *Exp. Fluids* **58** (2017), no. 75, article no. 75.
- [40] A. K. Banerjee, A. Bhattacharya and S. Balasubramanian, “Experimental study of rotating convection in the presence of bi-directional thermal gradients with localized heating”, *AIP Adv.* **8** (2018), no. 11, article no. 115324.
- [41] A. Sukhanovskii, E. Popova and A. Vasiliev, “A shallow layer laboratory model of large-scale atmospheric circulation”, *Geophys. Astrophys. Fluid Dyn.* **117** (2023), no. 3, pp. 155–176.
- [42] P. L. Read, P. Maubert, A. Randriamampianina and W.-G. Früh, “Direct numerical simulation of transitions towards structural vacillation in an air-filled, rotating, baroclinic annulus”, *Phys. Fluids* **20** (2008), no. 4, article no. 044107.
- [43] T. von Larcher, S. Viazzo, U. Harlander, M. Vincze and A. Randriamampianina, “Instabilities and small-scale waves within the Stewartson layers of a thermally driven rotating annulus”, *J. Fluid Mech.* **841** (2018), pp. 380–407.
- [44] P. L. Read, “A combined laboratory and numerical study of heat transport by baroclinic eddies and axisymmetric flows”, *J. Fluid Mech.* **489** (2003), pp. 301–323.
- [45] J. Pedlosky, *Geophysical Fluid Dynamics*, second edition, Springer, 1987.
- [46] R. T. Pierrehumbert and K. L. Swanson, “Baroclinic Instability”, *Ann. Rev. Fluid Mech.* **27** (1995), pp. 419–467.
- [47] G. K. Vallis, *Atmospheric and Oceanic Fluid Dynamics. Fundamentals and Large-scale Circulation*, Cambridge University Press, 2006.
- [48] M. E. McIntyre, “Diffusive destabilization of the baroclinic circular vortex”, *Geophys. Fluid Dyn.* **1** (1970), pp. 19–58.
- [49] V. I. Arnold, “On the conditions of nonlinear stability of plane stationary curvilinear currents of ideal fluids”, *Dokl. Akad. Nauk SSSR* **162** (1965), no. 5, pp. 975–978.
- [50] W. Blumen, “On the stability of quasi-geostrophic flow”, *J. Atmos. Sci.* **25** (1968), no. 5, pp. 929–931.
- [51] L. A. Diky and M. V. Kurgansky, “Integral conservation law for perturbations of zonal flow, and its applications to stability studies”, *Izv. - Atmos. Ocean. Phys.* **7** (1971), no. 9, pp. 623–626.
- [52] M. V. Kurgansky, *Adiabatic invariants in large-scale atmospheric dynamics*, Taylor & Francis, 2002, p. 222.
- [53] M. V. Kalashnik, M. V. Kurgansky and O. G. Chkhetiani, “Baroclinic instability in geophysical fluid dynamics”, *Physics - Uspekhi* **65** (2022), no. 10, pp. 1039–1070.
- [54] J. G. Charney and M. E. Stern, “On the stability of internal baroclinic jets in a rotating atmosphere”, *J. Atmos. Sci.* **19** (1962), pp. 159–172.
- [55] J. Pedlosky, “The Stability of Currents in the Atmosphere and the Ocean: Part I”, *J. Atmos. Sci.* **21** (1964), no. 2, pp. 201–219.
- [56] H. C. Davies and C. H. Bishop, “Eady edge waves and rapid development”, *J. Atmos. Sci.* **51** (1994), no. 13, pp. 1930–1946.
- [57] E. Heifetz, C. H. Bishop, B. J. Hoskins and J. Methven, “The counter-propagating Rossby-wave perspective on baroclinic instability. I: Mathematical basis”, *Q. J. R. Meteorol. Soc.* **130** (2004), no. 596, pp. 211–231.
- [58] E. Heifetz and J. Methven, “Relating optimal growth to counterpropagating Rossby waves in shear instability”, *Phys. Fluids* **17** (2005), article no. 064107.
- [59] B. F. Farrell and P. J. Ioannou, “Generalized Stability Theory. Part I: Autonomous Operators”, *J. Atmos. Sci.* **53** (1996), no. 14, pp. 2025–2040.
- [60] S. Chandrasekhar, *Hydrodynamic and Hydromagnetic Stability*, Oxford University Press, 1961.
- [61] V. Barcilon, “Role of the Ekman friction in the stability of the symmetric regime obtained in a rotating annulus”, *J. Atmos. Sci.* **21** (1964), pp. 291–299.
- [62] G. P. Williams and J. B. Robinson, “Generalized Eady waves and Ekman pumping”, *J. Atmos. Sci.* **31** (1974), pp. 1768–1776.
- [63] J. S. A. Green, “A problem in baroclinic stability”, *Q. J. R. Meteorol. Soc.* **86** (1960), no. 368, pp. 237–251.
- [64] W. Blumen, “Uniform potential vorticity flow: Part I—Theory of wave interactions and two-dimensional turbulence”, *J. Atmos. Sci.* **35** (1978), pp. 774–783.
- [65] M. Held, R. T. Pierrehumbert, S. T. Garner and K. L. Swanson, “Surface quasi-geostrophic dynamics”, *J. Fluid Mech.* **282** (1995), pp. 1–20.
- [66] N. A. Phillips, “A simple three-dimensional model for the study of large-scale flow patterns”, *J. Atmos. Sci.* **8** (1951), pp. 381–394.
- [67] E. N. Lorenz, “The mechanics of vacillation”, *J. Atmos. Sci.* **20** (1963), no. 3, pp. 448–465.
- [68] B. M. Boubnov and G. S. Golitsyn, *Convection in Rotating Fluids*, Kluwer Academic Publishers, 1995.
- [69] B. J. Hoskins, “The role of potential vorticity in symmetric stability and instability”, *Q. J. R. Meteorol. Soc.* **100** (1974), pp. 480–482.

- [70] T. J. Dunkerton, "On the inertial stability of the equatorial middle atmosphere", *J. Atmos. Sci.* **38** (1981), pp. 2354–2364.
- [71] P. D. Williams, P. L. Read and T. W. N. Haine, "Testing the limits of quasi-geostrophic theory: application to observed laboratory flows outside the quasi-geostrophic regime", *J. Fluid Mech.* **649** (2010), pp. 187–203.
- [72] B. P. Hignett, A. A. White, R. D. Carter, W. D. N. Jackson and R. M. Small, "A comparison of laboratory measurements and numerical simulations of baroclinic wave flows in a rotating cylindrical annulus", *Q. J. R. Meteorol. Soc.* **111** (1985), no. 467, pp. 131–154.
- [73] J. P. McGuirk and E. R. Reiter, "A vacillation in atmospheric energy parameters", *J. Atmos. Sci.* **33** (1976), no. 11, pp. 2079–2093.
- [74] L. Barry, G. Craig and J. Thuburn, "Poleward heat transport by the atmospheric heat engine", *Nature* **415** (2002), pp. 774–777.
- [75] M. Bowden and H. F. Eden, "Thermal Convection in a Rotating Fluids Annulus: Temperature, Heat Flow and Flow Field Observations in the Upper Symmetric Regime", *J. Atmos. Sci.* **22** (1965), no. 2, pp. 185–195.
- [76] E. Pérez-Pérez, P. L. Read and I. M. Moroz, "Assessing eddy parameterization schemes in a differentially heated rotating annulus experiment", *Ocean Model.* **32** (2010), no. 3, pp. 118–131. The magic of modelling: A special volume commemorating the contributions of Peter D. Killworth – Part 2.
- [77] R. L. Pfeffer, G. Buzyna and R. Kung, "Time-Dependent Modes of Behavior of Thermally Driven Rotating Fluids", *J. Atmos. Sci.* **37** (1980), no. 10, pp. 2129–2149.
- [78] M. Bowden and H. F. Eden, "Effect of a radial barrier on the convective flow in a rotating fluid annulus", *J. Geophys. Res. (1896-1977)* **73** (1968), no. 22, pp. 6887–6895.
- [79] Q. G. Rayer, D. W. Johnson and R. Hide, "Thermal convection in a rotating fluid annulus blocked by a radial barrier", *Geophys. Astrophys. Fluid Dyn.* **87** (1998), no. 3-4, pp. 215–252.
- [80] M. Vincze, T. Bozóki, M. Herein, et al., "The Drake Passage opening from an experimental fluid dynamics point of view", *Sci. Rep.* **11** (2021), article no. 19951.
- [81] G. P. Williams, "Baroclinic annulus waves", *J. Fluid Mech.* **49** (1971), no. 3, pp. 417–449.
- [82] B. Gallet and R. Ferrari, "The vortex gas scaling regime of baroclinic turbulence", *Proc. Natl. Acad. Sci. USA* **117** (2020), no. 9, pp. 4491–4497.
- [83] B. Gallet, B. Miquel, G. Hadjerici, K. J. Burns, G. R. Flierl and R. Ferrari, "Transport and emergent stratification in the equilibrated Eady model: the vortex-gas scaling regime", *J. Fluid Mech.* **948** (2022), article no. A31.
- [84] U. Achatz, M. J. Alexander, E. Becker, et al., "Atmospheric Gravity Waves: Processes and Parameterization", *J. Atmos. Sci.* **81** (2024), no. 2, pp. 237–262.
- [85] R. Hide, "Some experiments on thermal convection in a rotating liquid", *Q. J. R. Meteorol. Soc.* **79** (1953), no. 339, pp. 161–161.
- [86] R. L. Pfeffer and Y. Chiang, "Two kinds of vacillation in rotating laboratory experiments", *Mon. Wea. Rev.* **95** (1967), no. 2, pp. 75–82.
- [87] K. Ukajil and K. Tamaki, "A Numerical Study of Tilted-Trough Vacillation Observed in a Differentially Heated Rotating Fluid Annulus", *J. Meteorol. Soc. Jpn. Ser. II* **68** (1990), no. 4, pp. 447–460.
- [88] W. W. Fowles and R. L. Pfeffer, "Characteristics of Amplitude Vacillation in a Rotating, Differentially Heated Fluid Determined by a Multi-Probe Technique", *J. Atmos. Sci.* **26** (1969), no. 1, pp. 100–108.
- [89] J. E. Hart, "Finite Amplitude Baroclinic Instability", *Ann. Rev. Fluid Mech.* **11** (1979), no. 1, pp. 147–172.
- [90] B. G. Hunt, "Atmospheric Vacillations in a General Circulation Model I: The Large-Scale Energy Cycle", *J. Atmos. Sci.* **35** (1978), no. 7, pp. 1133–1143.
- [91] J. Pedlosky, "Finite-Amplitude Baroclinic Waves", *J. Atmos. Sci.* **27** (1970), no. 1, pp. 15–30.
- [92] P. E. Merelees, "On the periods of amplitude vacillations", *J. Meteorol. Soc. Jpn. Ser. II* **50** (1972), pp. 214–225.
- [93] K. Ohkitani and T. Sakajo, "Oscillatory damping in long-time evolution of the surface quasi-geostrophic equations with generalized viscosity: a numerical study", *Nonlinearity* **23** (2010), no. 12, article no. 3029.
- [94] J. Pedlosky, "Finite-Amplitude Baroclinic Waves with Small Dissipation", *J. Atmos. Sci.* **28** (1971), no. 4, pp. 587–597.
- [95] A. Barcilon and P. G. Drazin, "A Weakly Nonlinear Theory of Amplitude Vacillation and Baroclinic Waves", *J. Atmos. Sci.* **41** (1984), no. 22, pp. 3314–3330.
- [96] B. Wang and A. Barcilon, "The Weakly Nonlinear Dynamics of a Planetary Green Mode and Atmospheric Vacillation", *J. Atmos. Sci.* **43** (1986), no. 12, pp. 1275–1287.
- [97] J. Pedlosky and J. Thomson, "Baroclinic instability of time-dependent currents", *J. Fluid Mech.* **490** (2003), pp. 189–215.
- [98] M. C. Nguyen, M. J. Reeder, N. E. Davidson, R. K. Smith and M. T. Montgomery, "Inner-core vacillation cycles during the intensification of Hurricane *Katrina*", *Q. J. R. Meteorol. Soc.* **137** (2011), no. 657, pp. 829–844.
- [99] M. Vincze, U. Harlander, T. von Larcher and C. Egbers, "An experimental study of regime transitions in a differentially heated baroclinic annulus with flat and sloping bottom topographies", *Nonlinear Process. Geophys.* **21** (2014), no. 1, pp. 237–250.

- [100] S. H. Risch and P. L. Read, "A laboratory study of global-scale wave interactions in baroclinic flow with topography II: vacillations and low-frequency variability", *Geophys. Astrophys. Fluid Dyn.* **109** (2015), no. 4, pp. 359–390.
- [101] R. M. B. Young and P. L. Read, "Predictability of the thermally driven laboratory rotating annulus", *Q. J. R. Meteorol. Soc.* **142** (2016), no. 695, pp. 911–927.
- [102] S. C. Hardiman, A. A. Scaife, N. J. Dunstone and L. Wang, "Subseasonal Vacillations in the Winter Stratosphere", *Geophys. Res. Lett.* **47** (2020), no. 9, article no. e2020GL087766.
- [103] P. L. Read, "Rotating Annulus Flows and Baroclinic Waves", in *Rotating fluids in Geophysical and Industrial Applications* (E. J. Hopfinger, ed.), Springer, 1992, pp. 185–214.
- [104] R. H. Kraichnan, "Inertial ranges in two-dimensional turbulence", *Phys. Fluids* **10** (1967), pp. 1417–1423.
- [105] P. G. Saffman, "On the spectrum and decay of random two-dimensional vorticity distributions at large Reynolds number", *Stud. Appl. Math.* **50** (1971), no. 4, pp. 377–383.
- [106] R. D. Wordsworth, P. L. Read and Y. H. Yamazaki, "Turbulence, waves, and jets in a differentially heated rotating annulus experiment", *Phys. Fluids* **20** (2008), no. 12, article no. 126602.
- [107] C. Rodda and U. Harlander, "Transition from Geostrophic Flows to Inertia–Gravity Waves in the Spectrum of a Differentially Heated Rotating Annulus Experiment", *J. Atmos. Sci.* **77** (2020), no. 8, pp. 2793–2806.
- [108] P. J. Mason, "Baroclinic waves in a container with sloping end walls", *Philos. Trans. R. Soc. Lond., Ser. A* **278** (1975), no. 1284, pp. 397–445.
- [109] S. Condie and P. Rhines, "A convective model for the zonal jets in the atmospheres of Jupiter and Saturn", *Nature* **367** (1994), pp. 711–713.
- [110] P. L. Read, T. N. L. Jacoby, P. H. T. Rogberg, et al., "An experimental study of multiple zonal jet formation in rotating, thermally driven convective flows on a topographic beta-plane", *Phys. Fluids* **27** (2015), no. 8, article no. 085111.
- [111] A. M. Treguier, N. G. Hogg, M. Maltrud, K. Speer and V. Thierry, "The Origin of Deep Zonal Flows in the Brazil Basin", *J. Phys. Oceanogr.* **33** (2003), no. 3, pp. 580–599.
- [112] H. Nakano and N. Suginoara, "Importance of the eastern Indian Ocean for the abyssal Pacific", *J. Geophys. Res. Oceans* **107** (2002), no. C12, pp. 12-1–12-14.
- [113] R. Herbei, I. W. McKeague and K. G. Speer, "Gyres and Jets: Inversion of Tracer Data for Ocean Circulation Structure", *J. Phys. Oceanogr.* **38** (2008), no. 6, pp. 1180–1202.
- [114] D. Lemasquerier, B. Favier and M. M. Le Bars, "Zonal jets at the laboratory scale: hysteresis and Rossby waves resonance", *J. Fluid Mech.* **910** (2021), article no. A18.
- [115] H. Aref, "The development of chaotic advection", *Phys. Fluids* **14** (2002), no. 4, pp. 1315–1325.
- [116] A. S. Bower, "A Simple Kinematic Mechanism for Mixing Fluid Parcels across a Meandering Jet", *J. Phys. Oceanogr.* **21** (1991), no. 1, pp. 173–180.
- [117] R. M. Samelson and S. Wiggins, *Lagrangian Transport in Geophysical Jets and Waves*, Springer, 2006.
- [118] M. Agaoglou, V. J. García-Garrido, U. Harlander and A. M. Mancho, "Building transport models from baroclinic wave experimental data", *Phys. Fluids* **36** (2024), no. 1, article no. 016611.
- [119] R. Mizuta and S. Yoden, "Chaotic Mixing and Transport Barriers in an Idealized Stratospheric Polar Vortex", *J. Atmos. Sci.* **58** (2001), no. 17, pp. 2616–2629.
- [120] A. de la Cámara, C. R. Mechoso, A. M. Mancho, E. Serrano and K. Ide, "Isentropic Transport within the Antarctic Polar-Night Vortex: Rossby Wave Breaking Evidence and Lagrangian Structures", *J. Atmos. Sci.* **70** (2013), no. 9, pp. 2982–3001.
- [121] M. Abalos and A. de la Cámara, "Twenty-First Century Trends in Mixing Barriers and Eddy Transport in the Lower Stratosphere", *Geophys. Res. Lett.* **47** (2020), no. 21, article no. e2020GL089548.
- [122] M. E. McIntyre, "On the Antarctic ozone hole", *J. Atmos. Sol.-Terr. Phys.* **51** (1989), no. 1, pp. 29–43. Cedar Science-Part II.
- [123] G. García-Sánchez, A. M. Mancho, A. G. Ramos, J. Coca and S. Wiggins, "Structured pathways in the turbulence organizing recent oil spill events in the Eastern Mediterranean", *Sci. Rep.* **12** (2022), no. 1, article no. 3662.
- [124] G. Haller, *Transport Barriers and Coherent Structures in Flow Data*, Cambridge University Press, 2023.
- [125] J. Sommeria, S. Mayers and H. L. Swinney, "Laboratory model of a planetary eastward jet", *Nature* **337** (1989), pp. 58–61.
- [126] R. P. Behringer, S. D. Meyers and H. L. Swinney, "Chaos and mixing in a geostrophic flow", *Phys. Fluids, A* **3** (1991), no. 5, pp. 1243–1249.
- [127] S. Sugata and S. Yoden, "Chaotic Lagrangian Motion and Heat Transport in a Steady, Baroclinic Annulus Wave", *J. Meteorol. Soc. Jpn. Ser. II* **72** (1994), no. 4, pp. 569–587.
- [128] T. Tajima, T. Nakamura and T. Kuroda, "Laboratory Experiments of Lagrangian Motions in a Steady Baroclinic Wave - Internal Structures of Vortices-", *J. Meteorol. Soc. Jpn.* **73** (1995), no. 1, pp. 37–46.
- [129] T. Tajima and T. Nakamura, "Meridional Flow Field of Axisymmetric Flows in a Rotating Annulus", *J. Atmos. Sci.* **57** (2000), no. 18, pp. 3109–3121.

- [130] R. J. Keane, P. L. Read and G. P. King, “On the stirring properties of the thermally-driven rotating annulus”, *Phys. D: Nonlinear Phenom.* **268** (2014), pp. 50–58.
- [131] C. Mendoza and A. M. Mancho, “Hidden Geometry of Ocean Flows”, *Phys. Rev. Lett.* **105** (2010), no. 3, article no. 038501.
- [132] A. M. Mancho, S. Wiggins, J. Curbelo and C. Mendoza, “Lagrangian descriptors: A method for revealing phase space structures of general time dependent dynamical systems”, *Commun. Nonlinear Sci. Numer. Simul.* **18** (2013), no. 12, pp. 3530–3557.
- [133] I. M. Jánosi, P. Kiss, V. Homonnai, et al., “Dynamics of passive tracers in the atmosphere: Laboratory experiments and numerical tests with reanalysis wind fields”, *Phys. Rev. E* **82** (2010), no. 4, article no. 046308.
- [134] G. J. Shutts, “The propagation of eddies in diffluent jetstreams: Eddy vorticity forcing of ‘blocking’ flow fields”, *Q. J. R. Meteorol. Soc.* **109** (1983), no. 462, pp. 737–761.
- [135] P. Martineau, H. Nakamura, A. Yamamoto and Y. Kosaka, “Baroclinic blocking”, *Geophys. Res. Lett.* **49** (2022), article no. e2022GL097791.
- [136] J. G. Charney and D. M. Straus, “Form-drag instability, multiple equilibria and propagating planetary waves in baroclinic, orographically forced, planetary wave systems”, *J. Atmos. Sci.* **37** (1980), no. 6, pp. 1157–1176.
- [137] J. G. Charney and J. G. DeVore, “Multiple flow equilibria in the atmosphere and blocking”, *J. Atmos. Sci.* **36** (1979), no. 7, pp. 1205–1216.
- [138] A. R. Hansen and T.-C. Chen, “A Spectral Energetics Analysis of Atmospheric Blocking”, *Mon. Wea. Rev.* **110** (1982), no. 9, pp. 1146–1165.
- [139] D. F. Rex, “Blocking action in the middle troposphere and its effect upon regional climate. I An aerological study of blocking action”, *Tellus* **2** (1950), no. 3, pp. 196–211.
- [140] P. M. Sousa, D. Barriopedro, R. García-Herrera, T. Woollings and R. M. Trigo, “A new combined detection algorithm for blocking and subtropical ridges”, *J. Climate* **34** (2021), no. 18, pp. 7735–7758.
- [141] A. M. Obukhov, M. V. Kurgansky and M. S. Tatarskaya, “Dynamic conditions for the origin of droughts and other large-scale weather anomalies”, *Meteorol. Gidrol. (in Russian)* **10** (1984), pp. 5–13.
- [142] T. Kuhlbrodt and P. Névir, “Low-order point vortex models of atmospheric blocking”, *Meteorol. Atmos. Phys.* **73** (2000), pp. 127–138.
- [143] A. Müller, P. Nevir, L. Schielicke, M. Hirt, J. Pueltz and I. Sonntag, “Applications of point vortex equilibria: blocking events and the stability of the polar vortex”, *Tellus A* **67** (2015), article no. 29184.
- [144] G. Gottwald and R. Grimshaw, “The formation of coherent structures in the context of blocking”, *J. Atmos. Sci.* **56** (1999), pp. 3640–3662.
- [145] E. N. Lorenz, *The Nature and Theory of the General Circulation of the Atmosphere*, World Meteorological Organization, 1967, p. 161.
- [146] C.-G. Rossby, “On the dynamics of certain types of blocking waves”, *J. Chin. Geophys. Soc.* **2** (1950), pp. 1–13.
- [147] M. Kageyama, F. D’Andrea, G. Ramstein, P. J. Valdes and R. Vautard, “Weather regimes in past climate atmospheric general circulation model simulations”, *Clim. Dyn.* **15** (1999), pp. 773–793.
- [148] E. Moreno-Chamarro, D. Zanchettin, K. Lohmann, J. Luterbacher and J. H. Jungclauss, “Winter amplification of the European Little Ice Age cooling by the subpolar gyre”, *Sci. Rep.* **7** (2017), article no. 9981.
- [149] J. A. Francis and S. J. Vavrus, “Evidence for a wavier jet stream in response to rapid Arctic warming”, *Environ. Res. Lett.* **10** (2015), article no. 014005.
- [150] T. Woollings, D. Barriopedro, J. Methven, et al., “Blocking and its response to climate change”, *Curr. Clim. Change Rep.* **4** (2018), pp. 287–300.
- [151] I. I. Mokhov and A. V. Timazhev, “Atmospheric blocking and changes in its frequency in the 21st century simulated with the ensemble of climate models”, *Russ. Meteorol. Hydrol.* **44** (2019), no. 6, pp. 369–377.
- [152] M. V. Kurgansky, “A simple model of blocking action over a hemisphere”, *Theor. Appl. Climatol.* **147** (2022), pp. 65–71.
- [153] W. Moon, G. E. Manucharyan and H. A. Dijkstra, “Baroclinic instability and large-scale wave propagation in a planetary-scale atmosphere”, *Q. J. R. Meteorol. Soc.* **148** (2022), pp. 809–825.
- [154] N. A. Phillips, “Geostrophic motion”, *Rev. Geophys.* **1** (1963), no. 2, pp. 123–176.
- [155] E. R. Weeks, Y. Tian, J. S. Urbach, K. Ide, H. L. Swinney and M. Ghil, “Transitions Between Blocked and Zonal Flows in a Rotating Annulus with Topography”, *Science* **278** (1997), no. 5343, pp. 1598–1601.
- [156] R. W. Griffiths and P. F. Linden, “Intermittent baroclinic instability and fluctuations in geophysical circulations”, *Nature* **316** (1985), no. 2, pp. 801–803.
- [157] P. L. Read and S. H. Risch, “A laboratory study of global-scale wave interactions in baroclinic flow with topography I: multiple flow regimes”, *Geophys. Astrophys. Fluid Dyn.* **105** (2011), no. 2–3, pp. 128–160.
- [158] S. D. Marshall and P. L. Read, “An experimental investigation into topographic resonance in a baroclinic rotating annulus”, *Geophys. Astrophys. Fluid Dyn.* **109** (2015), no. 4, pp. 391–421.
- [159] S. D. Marshall and P. L. Read, “Thermal versus mechanical topography: an experimental investigation in a rotating baroclinic annulus”, *Geophys. Astrophys. Fluid Dyn.* **114** (2020), no. 6, pp. 763–797.

- [160] M. Rantanen, A. Y. Karpechko, A. Lipponen, et al., “The Arctic has warmed nearly four times faster than the globe since 1979”, *Commun. Earth Environ.* **3** (2022), no. 1, article no. 168.
- [161] B. Gyüre, I. Bartos and I. M. Jánosi, “Nonlinear statistics of daily temperature fluctuations reproduced in a laboratory experiment”, *Phys. Rev. E* **76** (2007), no. 3, article no. 037301.
- [162] F. J. Romeiras, C. Grebogi and E. Ott, “Multifractal properties of snapshot attractors of random maps”, *Phys. Rev. A* **41** (1990), no. 2, pp. 784–799.
- [163] M. Ghil, M. D. Chekroun and E. Simonnet, “Climate dynamics and fluid mechanics: Natural variability and related uncertainties”, *Phys. D: Nonlinear Phenom.* **237** (2008), no. 14–17, pp. 2111–2126.
- [164] M. Vincze, I. D. Borcia and U. Harlander, “Temperature fluctuations in a changing climate: an ensemble-based experimental approach”, *Sci. Rep.* **7** (2017), no. 1, p. 254.
- [165] C. Rodda, U. Harlander and M. Vincze, “Jet stream variability in a polar warming scenario – a laboratory perspective”, *Weather Clim. Dynam.* **3** (2022), pp. 937–950.
- [166] R. Geen, S. I. Thomson, J. A. Screen, et al., “An Explanation for the Metric Dependence of the Midlatitude Jet-Waviness Change in Response to Polar Warming”, *Geophys. Res. Lett.* **50** (2023), no. 21, article no. e2023GL105132.
- [167] M. Vincze, C. Hancock, U. Harlander, C. Rodda and K. Speer, “Extreme temperature fluctuations in laboratory models of the mid-latitude atmospheric circulation”, *Sci. Rep.* **13** (2023), no. 1, article no. 20904.
- [168] U. Harlander, I. D. Borcia, M. Vincze and C. Rodda, “Probability distribution of extreme events in a baroclinic wave laboratory experiment”, *Fluids* **7** (2022), no. 8, article no. 274.
- [169] T. Bozóki, L. Czelnai, A. Horicsányi, A. Nyerges, A. Pál, J. Pálfi and M. Vincze, “Large-scale ocean circulation in the Southern Hemisphere with closed and open Drake Passage—A laboratory minimal model approach”, *Deep-Sea Res. II: Top. Stud. Oceanogr.* **160** (2019), pp. 16–24.
- [170] M. Vincze, T. Bozóki, M. Herein, et al., “The Drake Passage opening from an experimental fluid dynamics point of view”, *Sci. Rep.* **11** (2021), no. 1, article no. 19951.
- [171] T. N. L. Jacoby, P. L. Read, P. D. Williams and R. M. B. Young, “Generation of inertia–gravity waves in the rotating thermal annulus by a localised boundary layer instability”, *Geophys. Astrophys. Fluid Dyn.* **105** (2011), no. 2–3, pp. 161–181.
- [172] A. E. Gill and A. Davey, “Instabilities of a buoyancy-driven system”, *J. Fluid Mech.* **35** (1969), no. 4, pp. 775–798.
- [173] A. Randriamampianina and E. Crespo del Arco, “Inertia–gravity waves in a liquid-filled, differentially heated, rotating annulus”, *J. Fluid Mech.* **782** (2015), pp. 144–177.
- [174] F. Lott, H. Kelder and H. Teitelbaum, “A transition from Kelvin–Helmholtz instabilities to propagating wave instabilities”, *Phys. Fluids*, **A 4** (1992), no. 9, pp. 1990–1997.
- [175] L. Rayleigh, “On the dynamics of revolving fluids”, *Proc. R. Soc. Lond., Ser. A* **93**, (648) (1917), pp. 148–154. <http://rspa.royalsocietypublishing.org/content/93/648/148.full.pdf>.
- [176] J. E. Hart and S. Kittelman, “Instabilities of the sidewall boundary layer in a differentially driven rotating cylinder”, *Phys. Fluids* **8** (1996), no. 3, pp. 692–696.
- [177] B. R. Sutherland, U. Achatz, C. P. Caulfield and J. M. Klymak, “Recent progress in modeling imbalance in the atmosphere and ocean”, *Phys. Rev. Fluids* **4** (2019), no. 1, article no. 010501.
- [178] S. Borchert, U. Achatz and M. D. Fruman, “Gravity wave emission in an atmosphere-like configuration of the differentially heated rotating annulus experiment”, *J. Fluid Mech.* **758** (2014), pp. 287–311.
- [179] C. Rodda, S. Hien, U. Achatz and U. Harlander, “A new atmospheric-like differentially heated rotating annulus configuration to study gravity wave emission from jets and fronts”, *Exp. Fluids* **61** (2020), article no. 2.
- [180] P. D. Williams, P. L. Read and T. W. N. Haine, “Spontaneous generation and impact of inertia-gravity waves in a stratified, two-layer shear flow”, *Geophys. Res. Lett.* **30** (2003), no. 24, article no. 2255.
- [181] R. Ford, “Gravity wave radiation from vortex trains in rotating shallow water”, *J. Fluid Mech.* **281** (1994), pp. 81–118.
- [182] P. D. Williams, T. W. N. Haine and P. L. Read, “Inertia–Gravity Waves Emitted from Balanced Flow: Observations, Properties, and Consequences”, *J. Atmos. Sci.* **65** (2008), no. 11, pp. 3543–3556.
- [183] J.-B. Flór, H. Scolan and J. Gula, “Frontal instabilities and waves in a differentially rotating fluid”, *J. Fluid Mech.* **685** (2011), pp. 532–542.
- [184] D. O’sullivan and T. J. Dunkerton, “Generation of Inertia–Gravity Waves in a Simulated Life Cycle of Baroclinic Instability”, *J. Atmos. Sci.* **52** (1995), no. 21, pp. 3695–3716.
- [185] O. Bühler, J. Callies and R. Ferrari, “Wave–vortex decomposition of one-dimensional ship-track data”, *J. Fluid Mech.* **756** (2014), pp. 1007–1026.
- [186] Q. Li and E. Lindborg, “Weakly or Strongly Nonlinear Mesoscale Dynamics Close to the Tropopause?”, *J. Atmos. Sci.* **75** (2018), no. 4, pp. 1215–1229.
- [187] C. Rodda, I. D. Borcia, P. L. Gal, M. Vincze and U. Harlander, “Baroclinic, Kelvin and inertia-gravity waves in the barostrat instability experiment”, *Geophys. Astrophys. Fluid Dyn.* **112** (2018), no. 3, pp. 175–206.
- [188] P. G. Baines, *Topographic Effects in Stratified Flows*, second edition, Cambridge University Press, 2022.



- [189] P. Léard, B. Favier, P. Le Gal and M. Le Bars, “Coupled convection and internal gravity waves excited in water around its density maximum at 4°C”, *Phys. Rev. Fluids* **5** (2020), no. 2, article no. 024801.
- [190] V. Dorel, P. Le Gal and M. Le Bars, “Experimental study of the penetrative convection in gases”, *Phys. Rev. Fluids* **8** (2023), no. 10, article no. 103501.
- [191] S. Abide, S. Viazzo, U. Harlander, G. Meletti, I. Raspo and A. Randriamampianina, “On the influence of the heat transfer at the free surface of a thermally-driven rotating annulus”, 2024.
- [192] M. Vincze, S. Borcert, U. Achatz, et al., “Benchmarking in a rotating annulus: a comparative experimental and numerical study of baroclinic wave dynamics”, *Meteorol. Z.* **23** (2014), no. 6, pp. 611–635.
- [193] R. M. B. Young and P. L. Read, “Predictability of the thermally driven laboratory rotating annulus”, *Q. J. R. Meteorol. Soc.* **142** (2016), no. 695, pp. 911–927.
- [194] I. M. Held, “100 Years of Progress in Understanding the General Circulation of the Atmosphere”, *Meteor. Monogr.* **59** (2019), pp. 6.1–6.23.
- [195] G. I. Taylor, “VIII. Stability of a viscous liquid contained between two rotating cylinders”, *Philos. Trans. R. Soc. Lond., Ser. A* **223** (1923), no. 605-615, pp. 289–343.
- [196] R. M. Lueptow, R. Hollerbach and E. Serre, “Taylor–Couette and related flows on the centennial of Taylor’s Philosophical Transactions paper: part 1”, *Philos. Trans. R. Soc. Lond., Ser. A* **381** (2023), no. 2243, article no. 20220140.
- [197] R. Hollerbach, R. M. Lueptow and E. Serre, “Taylor–Couette and related flows on the centennial of Taylor’s seminal Philosophical Transactions paper: part 2”, *Philos. Trans. R. Soc. Lond., Ser. A* **381** (2023), no. 2246, article no. 20220359.
- [198] F. Exner, “Über die Bildung von Windhosen und Zyklonen”, *Sitzungs Ber. Akad. Wiss. Wien, Abt. IIa* **132** (1923), pp. 1–16.
- [199] D. Fultz, R. R. Long, G. V. Owens, W. Bohan, R. Kaylor and J. Weil, *Studies of thermal convection in a rotating cylinder with some implications for large-scale atmospheric motions*, Springer, 1959.
- [200] T. Dauxois, T. Peacock, P. Bauer, C. P. Caulfield, C. Cenedese, et al., “Confronting Grand Challenges in environmental fluid mechanics”, *Phys. Rev. Fluids* **6** (2021), no. 2, article no. 020501.
- [201] S. Abide, S. Viazzo, I. Raspo and A. Randriamampianina, “Higher-order compact scheme for high-performance computing of stratified rotating flows”, *Comput. Fluids* **174** (2018), pp. 300–310.
- [202] G. Meletti, S. Abide, S. Viazzo and U. Harlander, “A parameter study of strato-rotational low-frequency modulations: impacts on momentum transfer and energy distribution”, *Philos. Trans. R. Soc. Lond., Ser. A* **381** (2023), no. 2246, article no. 20220297.
- [203] T. Seelig, U. Harlander, R. Faulwetter and C. Egbers, “Irregularity and singular vector growth of the differentially heated rotating annulus flow”, *Theor. Comput. Fluid Dyn.* **27** (2013), no. 3, pp. 415–432.
- [204] M. Hoff, U. Harlander and C. Egbers, “Empirical singular vectors of baroclinic flows deduced from experimental data of a differentially heated rotating annulus”, *Meteorol. Z.* **23** (2015), no. 6, pp. 581–597.
- [205] P. J. Schmid, “Nonmodal Stability Theory”, *Ann. Rev. Fluid Mech.* **39** (2007), pp. 129–162.
- [206] B. R. Sutherland, T. Dauxois and T. Peacock, “Internal waves in laboratory experiments”, in *Modelling Atmospheric and Oceanic Flows: Insights from Laboratory Experiments and Numerical Simulations* (T. v. Larcher and P. D. Williams, eds.), American Geophysical Union, 2015, pp. 193–212.
- [207] T. Caudwell, J.-B. Flór and M. E. Negretti, “Convection at an isothermal wall in an enclosure and establishment of stratification”, *J. Fluid Mech.* **799** (2016), pp. 448–475.
- [208] A. Schröder and D. Schanz, “3D Lagrangian Particle Tracking in Fluid Mechanics”, *Ann. Rev. Fluid Mech.* **55** (2023), no. 1, pp. 511–540.
- [209] B. R. Sutherland, M. DiBenedetto, A. Kaminski and T. van den Bremer, “Fluid dynamics challenges in predicting plastic pollution transport in the ocean: A perspective”, *Phys. Rev. Fluids* **8** (2023), no. 7, article no. 070701.